Human CEACAM1-LF regulates lipid storage in HepG2 cells via fatty acid transporter CD36

Jennifer Chean[1], **Charng-Jui Chen**[1], **Gabriel Gugiu**[1], **Patty Wong**[1], **Seung Cha**[1], **Harry Li**[1], **Tung Nguyen**[1], **Supriyo Bhatticharya**[2], and **John E. Shively**[1,*]

From the [1]Department of Immunology and Theranostics, and [2]Department of Computational and Quantitative Medicine, Beckman Research Institute of City of Hope, Duarte, California, USA

Edited by Peter Cresswell

Carcinoembryonic antigen-related cell adhesion molecule 1 (CEACAM1) is expressed in the liver and secreted as biliary glycoprotein 1 (BGP1) via bile canaliculi (BCs). CEACAM1-LF is a 72 amino acid cytoplasmic domain mRNA splice isoform with two immunoreceptor tyrosine-based inhibitory motifs (ITIMs). Ceacam1$^{-/-}$ or Ser503Ala transgenic mice have been shown to develop insulin resistance and nonalcoholic fatty liver disease; however, the role of the human equivalent residue, Ser508, in lipid dysregulation is unknown. Human HepG2 hepatocytes that express CEACAM1 and form BC in vitro were compared with CEACAM1$^{-/-}$ cells and CEACAM1$^{-/-}$ cells expressing Ser508Ala null or Ser508Asp phosphorylation mimic mutations or to phosphorylation null mutations in the tyrosine ITIMs known to be phosphorylated by the tyrosine kinase Src. CEACAM1$^{-/-}$ cells and the Ser508Asp and Tyr520Phe mutants strongly retained lipids, while Ser508Ala and Tyr493Phe mutants had low lipid levels compared with wild-type cells, indicating that the ITIM mutants phenocopied the Ser508 mutants. We found that the fatty acid transporter CD36 was upregulated in the S508A mutant, coexpressed in BCs with CEACAM1, co-IPed with CEACAM1 and Src, and when downregulated via RNAi, an increase in lipid droplet content was observed. Nuclear translocation of CD36 associated kinase LKB1 was increased sevenfold in the S508A mutant versus CEACAM1$^{-/-}$ cells and correlated with increased activation of CD36-associated kinase AMPK in CEACAM1$^{-/-}$ cells. Thus, while CEACAM1$^{-/-}$ HepG2 cells upregulate lipid storage similar to Ceacam1$^{-/-}$ in murine liver, the null mutation Ser508Ala led to decreased lipid storage, emphasizing evolutionary changes between the CEACAM1 genes in mouse and humans.

The liver plays a central role in lipid homeostasis, including the production of bile that contains both cholesterol and phospholipids. Biliary glycoprotein 1 (BGP1) is the major protein of bile (1). BGP1, now known as CEACAM1 (2), is highly expressed on the membranes of hepatocytes and bile canaliculi (BC), and as a coreceptor of insulin receptor, is responsible for insulin clearance in portal circulation (3). Since

CEACAM1 binds to cholesterol in bile (4), is highly expressed in the intestinal tract (5), and is a homotypic cell adhesion molecule, it is likely that CEACAM1 plays a more general role in lipid homeostasis, from lipid uptake in the intestine to storage in the liver. Signaling of the cytoplasmic domain isoforms of CEACAM1-SF (short form, 12 amino acids) or CEACAM1-LF (long form, 72 amino acids) has been studied in epithelial cells (6), lymphocytes (7), endothelial cells (8), and hepatocytes (3). Importantly, both the short and long isoforms mediate homotypic cell adhesions that trigger G-actin and annexin A2 binding via cytoplasmic domain proximal residues Phe450 and Thr457 (9–12), allowing plasma membrane (PM) signaling platforms to interact via the cytoskeleton. The long isoform contains two immunoreceptor tyrosine inhibitory motifs (ITIMs) that inhibit inflammation (7). As predicted for tyrosines of ITIMs that are phosphorylated by Src kinases and recruit Src homology domain-2 containing tyrosine phosphatases SHP1/2 (13), CEACAM1-LF also is phosphorylated by Src kinases (14) and recruits SHP1/2 (15, 16). The recruitment of SHP2 to the insulin receptor (IR) in the liver has recently been shown responsible for IR downregulation and insulin resistance (17).

Ceacam1$^{-/-}$ mice are insulin-resistant and become increasingly obese with age and develop nonalcoholic fatty liver disease (NAFLD) even on normal chow (18). The Ceacam1 mutation Ser503Ala in transgenic mice had a similar phenotype to Ceacam1$^{-/-}$ mice, implying a negative regulatory function (19, 20). The mechanism of the Ser503Ala null mutation in mice was ascribed to modulation of insulin receptor internalization (3). However, the coexpression of wild-type Ceacam1 in the transgenic mice complicates the interpretation of the role of the Ser503A mutation since wild-type versus mutant expression levels were not measured. In the study of Sippel et al. (21), Ser503 in rat CEACAM1-LF was shown to be phosphorylated by PKC and was required for bile acid efflux, along with an effect on the ITIM residue Tyr488. This study is complicated based on three issues. The first is that transfections were performed in heterologous cells, not in hepatocytes, the most active transporters of bile acids. Subsequently, BSEP, NTCP, and OSTα/β were shown to perform these functions in the liver (22) and not CEACAM1. Second, the claimed ecto-ATPase activity of CEACAM1 in BCs (23) was

later shown to be due to NTPDase8 (24), not CEACAM1. The third was the demonstration that Ser503 was phosphorylated by PKC since it was stimulated by forskolin and inhibited by staurosporine (21), is unlikely in the case of human CEACAM1. While the amino sequence of rat CEACAM1-LF, preceding the critical Ser503 residue, indeed conforms to a PKC consensus sequence in rat (25), the critical basic residues are absent in humans (Fig. 1). In consideration of alternative kinases, the downstream sequences following the conserved Ser503 in rat and mouse or Ser508 in man conform to a GSK3β consensus sequence including the requirement for the priming phosphorylation site +4Ser (26, 27), conserved in 15/16 mammalian species sequenced (28). In our companion paper, we showed that when the cytoplasmic domain of CEACAM1-LF was phosphorylated on Ser512 by PKA, Ser508 became a substrate for GSK3β. Thus, it is likely that, in the course of evolution, the signaling kinases for CEACAM1 have changed along with the amino acid sequences among species.

These observations, as well as the many studies that show important differences between rodents and humans in hepatic lipid storage and obesity (29) led us to examine CEACAM1-LF signaling in a human hepatocyte model in which the human CEACAM1 gene is highly expressed, similar to the liver (30). We hypothesized that phosphorylation of Ser508, similar to the murine equivalent Ser503, regulated phosphorylation of tyrosines in the proximal and/or distal ITIMs. We further hypothesized that subsequent recruitment of SHP2 by the phosphorylated ITIMs would depend on which ITIM was phosphorylated. To evaluate our hypotheses, we selected HepG2 cells that highly express CEACAM1 (31, 32) and form BCs in vitro (33). We knocked out CEACAM1 by a Crispr/Cas9 approach and compared the phenotype to the parental cells, as well as the CEACAM1⁻/⁻ cell lines transfected with null and phosphorylation mimics of Ser508, and null mutants of the ITIMs. Given the importance of lipid storage dysregulation in the liver, we used lipid droplet formation with an emphasis on the role of the fatty acid (FA) transporter CD36 as a phenotypic readout for these cell lines.

The distribution of energy-rich fatty acids throughout the body is mediated by endothelial lipoprotein lipase that hydrolyzes triacyl glycerides (TAGs) of postprandial circulating chylomicrons and VLDL (34). The released FAs, especially the long-chain FAs, are transported into the heart, skeletal muscle, and hepatocytes primarily by the widely distributed and highly regulated CD36 receptor (35). Upon binding its many ligands, CD36 is phosphorylated by the Src kinase Fyn in the muscle (36) and platelets (37). Notably, CEACAM1-LF is also phosphorylated by Src kinases resulting in activation of its ITIMs (7). Similar to CEACAM1-LF, CD36 plays a prominent role in

hepatic insulin resistance and hepatosteatosis (38). Since transport of FAs (as opposed to inflammatory oxidized lipids) to tissues is an essential function, it is perhaps surprising that CD36 is often associated with inflammation (39) and steatosis (40). We hypothesized that CEACAM1-LF and CD36 are biochemically connected in hepatocytes, since the absence of CEACAM1 is involved in inflammation and hepatosteatosis, and its liver levels are reduced in obesity (41). Furthermore, genetic studies implicate CD36 in obesity (42) and regulation of bile acid levels (43). A recent study has linked CD36 protein levels in HepG2 cells to proprotein convertase subtilisin/kexin type 9 (PCSK9), in which CD36 directly associates with PCSK9 and is degraded by it in the proteasome (44). These data further connect CD36 to lipid storage since PCSK9 also regulates the levels of LDL receptor, a key lipid import receptor in the liver (45). In addition, CD36 has been shown to form a complex with AMPK and LKB1, and in the presence of FAs, leads to the activation of AMPK (46). Based on these observations, we also investigated the effect of CEACAM1 signaling on the expression of CD36 and its associated signaling proteins LKB1, Src, PCSK9, and AMPK.

Results

Generation of HepG2 CEACAM1⁻/⁻ (KO) cells and expression of CEACAM1-LF mutants in the KO cells

As stated above, HepG2 cells express high levels of CEACAM1-LF and form BC under ordinary culture conditions, two key features of human hepatocytes. CEACAM1 was genetically deleted from these cells by a CRISPR/Cas9 approach. Among the 30 sgRNAs tested, three directed at exon 4 gave surveyor nuclease treated DNA that showed fragmentation of the 806 kb exon 4 PCR fragment into smaller fragments (Fig. 2, A and B). Transfection of sgRNA 4.1 into HepG2 cells and FACS selection led to a CEACAM1⁻/⁻ cell line lacking CEACAM1 expression (Fig. 2C). Ser-508 in the cytoplasmic domain of CEACAM1-LF was mutated to either Ala (S508A, kinase null mutation) or Asp (S508D, phosphorylation mimic), as well as the Tyr null mutants Y493F and Y520F (Fig. 2D) were generated and transfected into the CEACAM1⁻/⁻ cell line. Immunoblot analysis of WT HepG2 cells shows high expression of human CEACAM1 compared with another reference line, Huh7, and absence of its expression in the genetically deleted line (Fig. 2E). Expression of the transfected mutants into the CEACAM1⁻/⁻ line compared with the WT cell line is shown in Figure 2F. The relative lower level expression of the mutants Y493F and Y520F is a reproducible phenotype for these mutants. Insulin treatment had little effect on the expression of the CEACAM1-LF mutants, an expected result in which expression is driven by a β-actin promoter.

Figure 1. CEACAM1 cytoplasmic domain sequence homology and conserved functional domains. Partial sequences of rat (Rno), mouse (Mmu), and human (Has) CEACAM1 sequences taken from Kammerer and Zimmermann (28). Conserved regions for β-catenin binding (85) in *blue*, for ITIMs in *green*, and for GSK3β in *red*. Key residues indicated in color. Double basic residues in rat preceding Ser503 *underlined*.
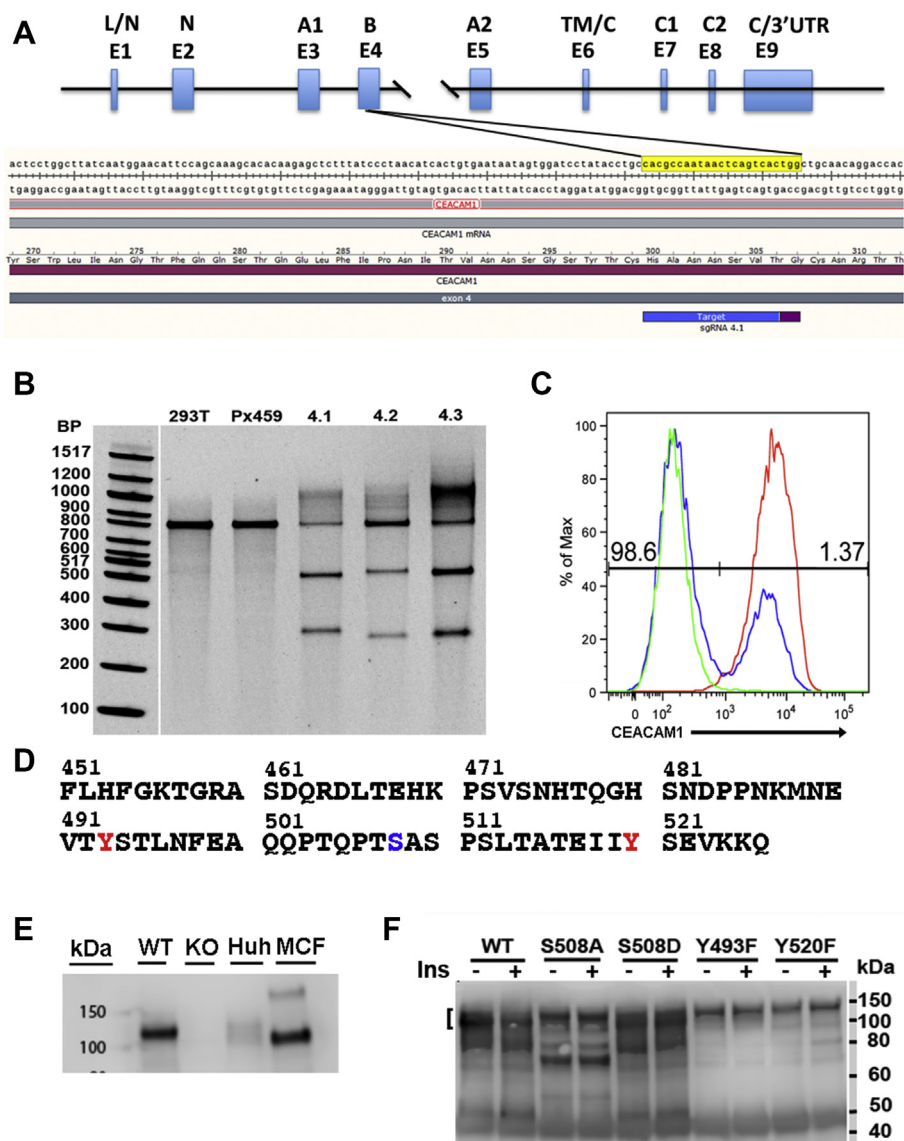
Figure 2. Generation of *CEACAM1*^−/−^ cells and expression of CEACAM1 mutants in *CEACAM1*^−/−^ HepG2 cells. *A*, exon structure of human *CEACAM1*, location of guide RNA sgRNA 4.1 and its target sequence in exon 4. *B*, surveyor nuclease restriction digest of DNA from untransfected 293T cells, vector control transfected 293T cells, and 293T cells transfected with sgRNA 4.1 to 4.3. *C*, enrichment of KO HepG2 cells for deletion of *CEACAM1* by negative selection. *Red trace* = WT HepG2 cells. *Blue trace* = sgRNA transfected cells prior to negative selection. *Green trace* = sgRNA transfected cells after negative selection of anti-CEACAM1 beads. *D*, sequence of human CEACAM1-LF cytoplasmic domain with key residues marked. *E*, immunoblot staining (20 μg of lysates per lane) for CEACAM1 in WT HepG2 and Huh7 (Huh) human hepatocyte cell lines, along with a CEACAM1-LF transfected cell line control (MCF). *F*, immunoblot staining (20 μg of lysates per lane) for CEACAM1 in HepG2 WT, and mutant Ser508A, Ser508D, Tyr493F, and Tyr520F transfected into the *CEACAM1*^−/−^ cells before and after treatment with insulin.

## Changes in total lipid, lipid droplet, and BC size in CEACAM1^−/−^ and mutant cells

When the cell lines were stained for lipid droplets with the fluorescent dye Vala, the trend was *CEACAM1*^−/−^ = S508D = Y520F > WT > S508A > Y493F (Fig. 3, *A–F*). Quantitation of the fluorescent staining (Fig. 3*G*) reveals a 60% increase in lipid staining in *CEACAM1*^−/−^ *versus* WT and an even greater increase in the S508D and Y520F mutants, 80% and 78%, respectively. The Y493F mutant had a 50% decrease in lipid droplet staining compared with WT cells, suggesting that abrogation of tyrosine phosphorylation at this site has a profound effect on lipid droplet storage. When a number of lipid droplets (LDs) per cell were analyzed according to large LDs (≥1 μm) *versus* small LDs (<1 μm) (Table 1 and Fig. S1), the lowest numbers of LDs were for WT = S508A or Y493F and highest number of LDs for *CEACAM1*^−/−^ = S508D or Y520F.

Immunostaining for CEACAM1 and F-actin (phalloidin) for BCs (Fig. 3, *H–M*) of WT cells demonstrated a predominant localization of BCs at the junctions of three cells (Fig. 3*H*). A similar F-actin staining pattern was seen for *CEACAM1*^−/−^ and WT cells, indicating that genetic ablation of *CEACAM1* did not affect BC formation (Fig. 3*H versus* Fig. 3*I*). In the case of the S508A mutant, BCs were enlarged with enhanced staining for CEACAM1 (Fig. 3*J*); however, BCs in the S508D mutant were of similar size to those in the WT cells (Fig. 3, *H* and *K*). The BC staining pattern for the tyrosine mutants (Fig. 3, *L* and *M*) revealed that the Y520F mutant was similar to WT cells and the S508D mutant, while the Y493F mutant was similar to
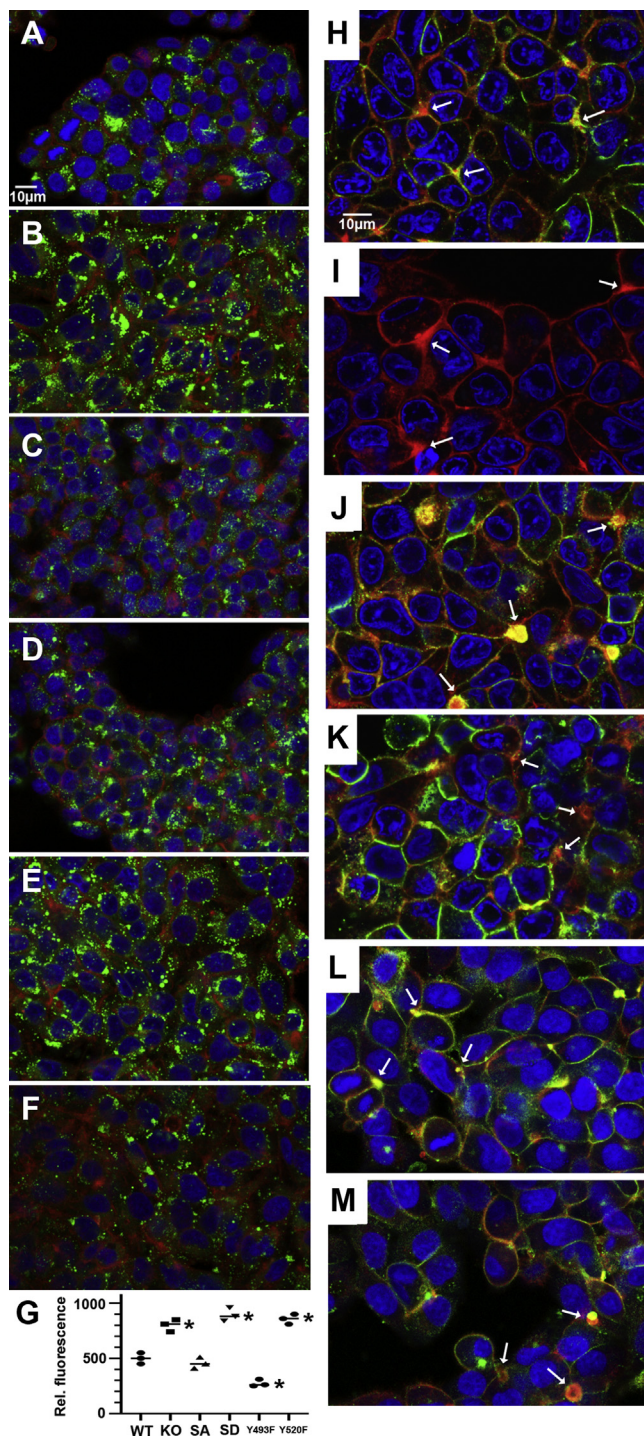
Figure 3. Effect of *CEACAM1^{−/−}* and mutant cell lines on lipid droplet staining and bile canaliculi formation for HepG2 cells. *A–F*, lipid droplet staining with Vala (*green*), nuclei (*blue*), and F-actin (*red*): *A*, WT. *B*, CEACAM1^{−/−}. *C–F*, CEACAM1^{−/−} transfected with S508A mutant (*C*), S508D mutant (*D*), Y520F mutant (*E*), and Y493F mutant (*F*). *G*, quantitation of lipid staining of the six cell lines (see Experimental procedures). *H–M*, staining with anti-CEACAM1 (*green*), F-actin (*red*), and nuclei (*blue*). *H*, WT. *I*, KO. *J–M*, KO transfected with S508A mutant (*J*), S508D mutant (*K*), Y520F mutant (*L*), and Y493F mutant (*M*). Magnification 40×, *arrows* indicated three representative BCs located at junctions of three cells.

the S508A mutant. Comparison of the lipid staining of the cell lines in Figure 3, *A–F* to the BC staining in Figure 3, *H–M* indicates a relationship between lipid content and BC size,

indicating that the lower lipid content of the S508A mutant is associated with the increased size of the BCs.

Comparative changes in lipid composition in CEACAM1 KO and mutant cells

LC/MS was used to determine if lipid composition was affected in the cell lines. The results were normalized to POPC, the most abundant phospholipid. The most abundant TAGs (*e.g.*, 16:0, 18:1, 18:1) were similar in all four cell lines (data not shown). In order to compare the effects of the *CEACAM1^{−/−}* and mutant cells *versus* WT cells, the results were reported as a ratio to WT (Table 2). Notably, 19 out of the 20 top upregulated lipids in the *CEACAM1^{−/−}* cells compared with the WT cells were TAGs, whereas only five of the top 20 downregulated lipids were TAGs. Only six of the top 20 upregulated lipids in the S508A mutant were TAGs, while 15 of the top 20 upregulated lipids in the S508D mutant were TAGs. Thus, the S508D mutant most closely resembles the *CEACAM1^{−/−}* cell line in lipid composition. In terms of the constituent FAs of the TAGs, 14/20 of the upregulated TAGs for the *CEACAM1^{−/−}* versus WT analysis had exclusively unsaturated FAs at all three positions, while only 3/20 had one unsaturated FAs in their TAGs. On the other hand, the five downregulated TAGs for the *CEACAM1^{−/−}* versus WT had only saturated FAs. Strikingly, 22:5 and 22:6 polyunsaturated FAs (PUFAs) predominated in the upregulated TAGs. Docosapentaenoic acid (22:5) and docosahexaenoic acid (22:6) are important omega-6 PUFAs that are precursors to prostaglandins and leukotrienes, important in the inflammatory response. Non-TAG lipids upregulated in the S508A mutant were phospholipids, suggesting that these are the lipids destined for efflux *via* enlarged BCs, since phospholipids, not TAGs, are a common component of bile (47).

CEACAM1-SF also reverses lipid droplet accumulation CEACAM1 KO cells

Since hepatocytes express both CEACAM1-LF and CEACAM-SF (48) by alternative mRNA splicing, it was important to determine if CEACAM-SF was also capable of restoring normal function to HepG2 KO cells. Accordingly, a cDNA encoding CEACAM1-SF was transfected into HepG2 KO cells and a cell line developed with high expression of CEACAM1-SF (Fig. 4, *A–C*). When these cells were stained for lipid droplets (Fig. 4D), lipid droplet numbers returned to WT levels and lipid staining was comparable to the levels seen in the S508A mutant transfected cells (Fig. 4E). These results suggest that both isoforms play roles in lipid droplet regulation in this hepatocyte model. In terms of functional analysis, we have previously shown that CEACAM1-SF is both necessary and sufficient to confer lumen formation on the breast epithelial cell line MCF7 either *in vitro* (49) or in an animal model of mammary gland formation (50). In terms of signal transduction mechanism, the 12 amino acid cytoplasmic domain of CEACAM1-SF shares the ability with CEACAM1-LF to interact with G-actin (50) and Annexin A2 (11), implicating roles for cytoskeleton formation at the PM. Although

Table 1
Lipid droplet sizes and number per cell for CEACAM1 WT, KO, and mutant HepG2 cell lines[a]

Size	WT	KO	S508A	S508D	Y493F	Y520F
≥1 μm	1.4 ± 1.5	5.3 ± 2.3 <0.001	1.9 ± 1.7 NS	3.6 ± 3.3 <0.001	2.0 ± 1.8 NS	5.4 ± 2.9 <0.001
<1 μm	5.7 ± 2.1	10.2 ± 4.3	10.4 ± 4.5	7.4 ± 3.4	5.4 ± 0.4	10.9 ± 0.8
p value		<0.001	<0.001	<0.01	NS	<0.001

[a] Cells were triple stained with Vala (lipid), DAPI (nuclei) and phalloidin (cell membrane). Lipid droplets (Vala) counted per cell (DAPI) were scored as ≥ or <1 μm and averaged for 50 cells. Repeat counts (three fields) were used to determine the standard deviations. Analysis of variance *versus* WT was performed with one-way ANOVA with a post hoc confidence interval of 95.

further studies on CEACAM1-SF are warranted, given the numerous studies on CEACAM1-LF signaling in rodent liver (51), the current study remains focused on CEACAM1-LF and its signaling domain mutants.

Expression of CD36 in lipid droplets and BC formation in CEACAM1^{−/−} and mutant cells

Since the import of FAs into the liver plays a major role in the development of fatty liver (42), we measured the expression of CD36, the FA transporter most relevant to the liver, as well as in muscle and adipose tissue (37). In addition, CD36 expression is directly involved in hepatosteatosis (38). CD36 staining exhibited the trend of S508A > S508D = CEACAM1^{−/−} = Y520F = Y493F > WT (Fig. 5, A–F). Quantitation of CD36

staining showed >threefold increase for CEACAM1^{−/−} *versus* WT and >ninefold for S508A *versus* WT (Fig. 5G). The highest CD36 expression was associated with the PM and BCs in the S508A mutant (Fig. 5H). Thus, the S508A mutant exhibited upregulation of CD36 and CD36 colocalized with BCs compared with WT cells in which CD36 expression was low. Downregulation of CD36 in the S508A mutant by CD36 RNAi reduced its expression and the number and size of BCs per microscopic field compared with RNAi control-treated cells (Fig. 5, I and J). CD36 and CEACAM1 colocalized at PMs and BCs in the S508A mutant (Fig. S2).

The effect of CD36 RNAi on lipid droplet formation was studied on high CD36 expressing Ser508 mutant cells. Lipid droplet formation increased after treatment of the S508A

Table 2
Analysis of CEACAM1^{−/−} and mutants compared with WT HepG2 cells[a]

Lipid	Log 2 [KO/WT]	Lipid	Log 2 [SA/WT]	Lipid	Log 2 [SD/WT]
TG(20:1_22:5_22:5)	8.31	PC(10:1e_16:1)	3.69	TG(18:1_22:6_22:6)	7.05
TG(18:1_22:6_22:6)	7.16	PC(18:1_14:2)	3.28	TG(18:2_14:1_17:1)	5.35
TG(18:1_22:4_22:5)	6.26	PG(16:0_18:1)	3.17	TG(16:1_22:6_22:6)	4.67
TG(16:1_22:6_22:6)	5.79	PI(18:1_20:3)	2.66	TG(14:0_22:6_22:6)	4.53
TG(16:1_22:5_22:6)	5.48	PC(26:1_18:1)	2.6	TG(16:1_22:5_22:6)	4.21
TG(14:0_22:6_22:6)	5.31	LPC(16:1e)	2.58	PC(10:1e_16:1)	3.85
TG(18:1_22:5_22:6)	5.21	PC(18:2e_18:0)	2.3	TG(14:0_17:1_22:6)	3.82
TG(16:0_22:5_22:6)	4.99	TG(14:0_17:1_22:6)	2.11	PC(18:1_14:2)	3.75
TG(18:1_20:3_22:6)	4.88	TG(16:0_18:1_22:6)	1.89	TG(18:1_20:3_22:6)	3.7
TG(20:1_22:5_22:6)	4.59	AcCa(17:1)	1.82	TG(20:1_22:5_22:6)	3.65
TG(20:1_22:4_22:5)	4.47	PE(20:4_21:1)	1.7	TG(14:0_22:5_22:6)	3.43
TG(14:0_22:5_22:6)	4.42	TG(16:1_22:6_22:6)	1.63	TG(20:1_22:5_22:5)	3.27
TG(22:0_22:5_22:5)	4.21	TG(18:0_16:0_22:6)	1.59	PE(15:0_22:6)	3.23
TG(14:0_17:1_22:6)	4.2	LPC(26:1)	1.25	PE(18:0_22:6)	3.21
PG(22:6_22:6)	4.01	PE(15:0_22:6)	1.23	TG(22:6_14:1_17:1)	3.16
TG(16:1_18:3_22:6)	3.95	TG(18:0_22:0_22:0)	1.22	TG(16:0_22:5_22:6)	3.12
TG(18:1_20:3_22:5)	3.7	PC(16:1_14:0)	1.16	TG(18:1_12:2_17:1)	3.1
TG(16:0_20:4_22:6)	3.69	PG(16:1_22:6)	1.08	PG(22:6_22:6)	3.09
TG(22:6_14:1_17:1)	3.66	TG(16:1_17:1_18:1)	0.92	TG(18:1_20:3_22:5)	3.06
TG(18:1_18:2_22:6)	3.51	PE(26:1_22:6)	0.91	TG(18:1_17:1_22:6)	3.05
PI(16:1_18:1)	−2.01	PC(10:0e_14:1)	−1.6	PS(16:0_20:5)	−3.66
PC(16:2e_22:0)	−2.02	DG(16:0_23:1)	−1.72	PS(16:0_16:1)	−3.72
TG(20:0e_16:0_16:1)	−2.05	Hex2Cer(d18:1_14:0+O)	−1.78	PI(16:0_16:1)	−3.74
Hex2Cer(d18:1_16:0+O)	−2.08	Hex2Cer(d18:1_14:0)	−1.81	PS(20:1_18:1)	−3.86
Cer(d18:1_16:1)	−2.1	PG(22:6_22:6)	−1.93	PI(18:0_22:6)	−3.92
PS(16:0_16:1)	−2.11	TG(26:1_18:1_22:6)	−1.94	PI(18:0_22:5)	−4.01
TG(20:0e_16:0_20:1)	−2.11	PI(16:1_16:1)	−2.13	PS(16:0_14:0)	−4.08
TG(20:0e_16:0_18:0)	−2.13	DG(26:1_16:0)	−2.13	PS(18:1_22:1)	−4.11
PS(20:1_18:1)	−2.18	LPC(18:1)	−2.23	PS(17:1_16:1)	−4.32
TG(20:0e_16:0_18:1)	−2.22	LPC(25:1)	−2.27	PC(18:3e_24:1)	−4.35
PS(18:1_18:1)	−2.4	ChE(30:6)	−2.38	PS(16:1_18:2)	−4.61
TG(16:0_18:1_18:1)	−2.43	PC(16:2e_22:0)	−2.39	PI(16:1_18:1)	−4.72
PC(14:0_14:1)	−2.56	PS(16:1_14:0)	−2.5	PS(16:1_16:1)	−5.11
PS(17:1_16:1)	−2.67	PS(14:0_14:0)	−2.51	PS(16:1_14:0)	−5.21
PC(16:1_14:1)	−2.81	PC(16:1_12:1)	−2.59	Hex2Cer(d18:1_16:0+O)	−5.38
PS(14:0_14:0)	−3.01	PC(18:3e_24:1)	−2.63	PS(16:1_22:6)	−5.72
PS(16:1_16:1)	−3.2	LPC(20:3)	−2.66	PS(18:0_22:4)	−5.72
PC(16:1_12:1)	−3.21	Hex2Cer(d18:1_16:0+O)	−3.07	Cer(d18:1_16:1)	−5.97
PI(16:1_16:1)	−3.44	Cer(d18:1_16:1)	−3.12	PS(14:0_14:0)	−6.06
PS(16:1_14:0)	−4.64	PI(18:0_22:6)	−3.82	PI(16:1_16:1)	−7.64

[a] Triacylglycerides (green), fold upregulated (red), fold downregulated (blue).

ASBMB

J. Biol. Chem. (2021) 297(5) 101311 **5**
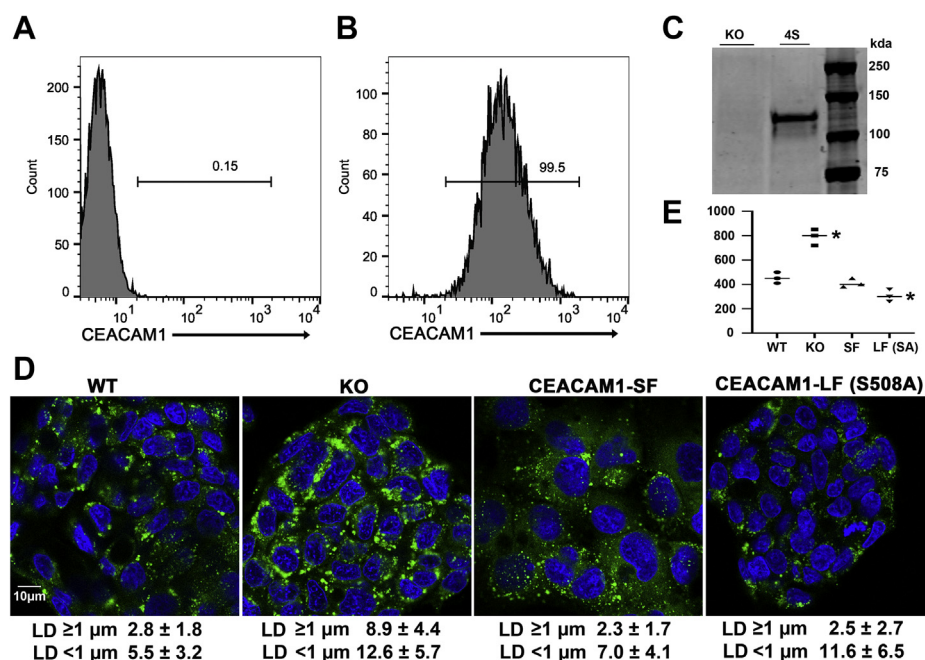
Figure 4. Expression of CEACAM1-SF in CEACAM1$^{-/-}$ HepG2 cells and lipid droplets. *A* and *B*, flow analysis of CEACAM1 KO cells before (*A*) and after (*B*) transfection with CEACAM1-SF. *C*, SDS gel analysis of CEACAM1 KO cells and CEACAM1 KO cells transfected with CEACAM1-SF (4S). *D*, comparative lipid droplet staining for WT, CEACAM1 KO, and CEACAM1 KO cells transfected with CEACAM1-SF or CEACAM1-LF (S508A mutant). *E*, quantitation of lipid droplet (LD) for two sizes per cell (see Experimental procedures) is shown below each panel.

mutant cells with CD36 RNAi (Fig. 5, *K–N*). Expression of CD36 mRNA by qRT-PCR (Fig. 5*O*) also showed S508A mutants expressed the highest levels of CD36, while after RNAi treatment, the mRNA levels were essentially undetectable (Fig. 5*P*). Flow analysis of cell surface levels of CD36 that show highest expression in S508A cells (Fig. 5*Q*) agrees with the confocal staining results (Fig. 5*C*). However, immunoblot staining for CD36 (Fig. 5*R*) is discordant, suggesting that this analysis is affected by the extraction of palmitylated CD36 from lipid raft microdomains (35). Thus, CD36 expression is downregulated by CEACAM1-LF signaling in WT cells, but in the S508A mutant where CEACAM1-LF phosphorylation is blocked, CD36 is upregulated and colocalized with CEACAM1-LF to BCs. When expression of CD36 in the S508A mutant was abrogated by RNAi, the number and size of BCs were dramatically reduced, leading to increased retention of lipid. Thus, lipid accumulation correlates with reduction of the number and size of BCs, which in turn depends on the expression of CD36. The S508A mutation led to not only high CD36 expression, but also to CD36 accumulation in BCs and low lipid droplet retention. We conclude that phosphorylation of Ser508 in CEACAM1-LF regulates CD36 expression, and that CD36 expression mediates the effects seen for CEACAM1-LF shown in Figure 3.

Association of CD36 with CEACAM1, LKB1, and Src

The low expression of CD36 in WT cells is likely regulated by coreceptors in addition to CEACAM1, since CD36 is found in a complex with the Src kinase Fyn, AMPK, and liver kinase B1 (LKB1) in muscle (46) and adipocytes (52), where Fyn

phosphorylation of LKB1 promotes its import into the nucleus preventing activation of AMPK. When CD36 binds FAs, it causes the dissociation of the complex, shifting the equilibrium toward cytosolic LKB1. The fact that *Cd36$^{-/-}$* mice have constitutively active AMPK in the heart and skeletal muscle is consistent with this pathway (46). To interrogate these CD36 associations in WT *versus CEACAM1$^{-/-}$* and the mutant cell lines, immunostaining was first performed for nuclear LKB1. Nuclear LKB1 staining revealed the following pattern: S508A (45 ± 10%) > WT (24 ±5%) > SD (14 ± 5%) > *CEACAM1$^{-/-}$* (6 ± 2%) (Fig. 6, *A–D*). Thus, compared with *CEACAM1$^{-/-}$* cells, the S508A mutant cells had a sevenfold increase in LKB1 nuclear localization and a twofold increase over WT cells. Costaining of the S508A mutant cells for LKB1 and CD36 revealed that CD36 was mainly confined to the PM while LKB1 was mainly nuclear (Fig. 6*E*). According to the CD36/LKB1/AMPK pathway in muscle (46), low nuclear LKB1 as observed in *CEACAM1$^{-/-}$* cells would be expected to compensate for their excess lipids by activating AMPK. Indeed, immunoblot analysis of the cell lines for activated AMPK (pT^{172}-AMPK) revealed the followed order: *CEACAM1$^{-/-}$* > S508A > WT = SD = Y493F > Y520F (Fig. 6*F*). Thus, *CEACAM1$^{-/-}$* cells had the lowest levels of nuclear LKB1 and highest levels of activated AMPK. Since NAFLD is known to trigger a compensatory pAMPK response (53), the high expression of pAMPK in *CEACAM1$^{-/-}$* cells that have high levels of lipid droplets is not unexpected.

CD36 protein levels have been shown to be regulated by PCSK9 in human HepG2 cells (44), similar to the regulation of LDLR by PCSK9 in hepatocytes (45). PCSK9 knockout mice fed a high-fat diet were found to have high levels of liver CD36 and lipid droplets, while knockdown of PCSK9 with shRNA in
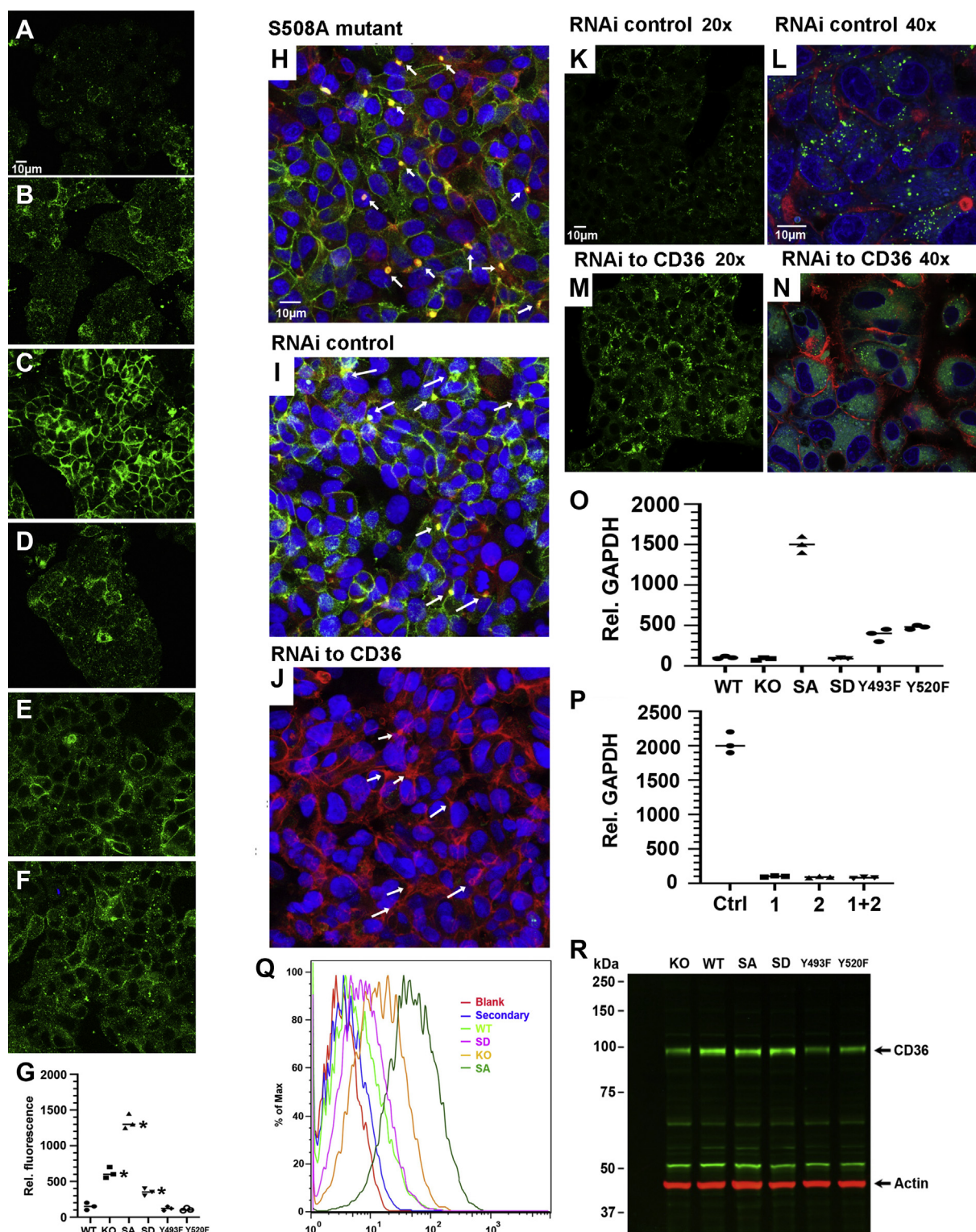
Figure 5. High CD36 expression in S508A mutant and effect of CD36 RNAi. *A–F*, staining of CD36 (*green*) in HepG2 cell lines. *G*, quantitation of CD36 staining for the six cell lines (see Experimental procedures). *H–J*, S508A mutants stained with CD36 (*green*), F-actin (*red*), and DAPI (*blue*). CD36 and BC expression of untreated (*H*) and RNAi control-treated (*I*) S508A mutant cells *versus* RNAi to CD36-treated S508A mutant cells (*J*). BCs are shown with *arrows*. *K–N*, lipid droplet staining (*green*) of S508A mutant cells. Control RNAi treatment at 20× (*K*) and 40× (*L*). RNAi to CD36 treatment at 20× (*M*) and 40× (*N*). *O*, mRNA expression levels in cell lines by qRT-PCR (in triplicate, relative to GAPDH). *P*, treatment of cell lines with no RNAi, control RNAi, RNAi-1, RNAi-2, and RNAi-1 plus RNAi-2 to CD36 (in triplicate, relative to GAPDH). *Q*, cell surface levels of CD36 on four cell lines. *R*, SDS gel analysis of CD36 expression in six cell lines. KO, knockout; SA, S508A mutant; SD, S508D mutant; WT, wild type.
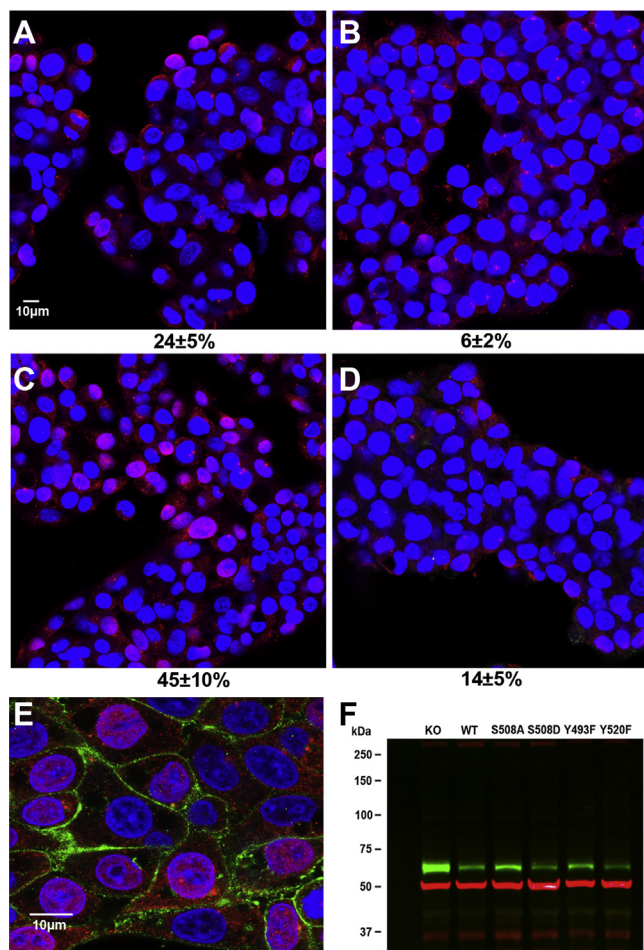
Figure 6. Nuclear expression of LKB1 in WT, CEACAM1⁻/⁻, and S508A and S508D mutants and AMPK expression. LKB1 nuclear expression in WT (*A*) and in CEACAM1⁻/⁻ (*B*) and in S508A (*C*) and S508D (*D*) mutants (*red* = LKB1, *blue* = DAPI). Percent LKB1 positive nuclei per 50 cells counted for three fields ±SEM shown underneath each panel. Magnification 20×. *E*, triple staining of S508A mutant for CD36 (*green*), LKB1 (*red*) and nuclei (*blue*). Magnification 40×. *F*, immunoblots for the detection of activated AMPK (*green channel*) in WT, CEACAM1 KO, and CEACAM1 mutants (tubulin in *red channel*). Twenty micrograms of protein lysate loaded per lane.

HepG2 cells resulted in high levels of CD36 and lipid droplet accumulation (54). It was concluded that high CD36 expression correlated with high lipid droplet accumulation in hepatocytes and that its degradation by PCSK9 was responsible for less lipid accumulation. In contrast, we found that the CEACAM1-LF S508A mutant in HepG2 cells had high expression of PM CD36 and low lipid droplet accumulation. To investigate this apparent contradiction, we knocked down PCSK9 with RNAi in the S508A mutant cells (Fig. 7). As expected PCSK9 expression was expressed in the cytoplasm for both WT and S508A mutant HepG2 cells (Fig. 7, *A* and *B*), but when the S508A mutant cells were treated with RNAi for PCSK9, quite unexpectedly, CD36 expression was dramatically reduced compared with control RNAi treated cells (Fig. 7, *C* and *D*). The reciprocal experiment in which CD36 was knocked down with RNAi and the cells stained for PCSK9 failed to reduce PCSK9 expression (Fig. 7, *E* and *F*), demonstrating that PCSK9 regulates CD36 protein levels, but not vice versa. The mRNA levels of PCSK9 as measured by qRT-PCR

were reduced to background by PCSK9 RNAi, while CD36 mRNA levels were reduced by about 50% (Fig. 7, *G* and *H*). Thus, CD36 expression is regulated by the interplay of PCSK9 (degradation pathway) and by CEACAM1-LF signaling (inhibition of degradation). This finding has similarities to the LDLR paradigm in which reduction of PCSK9 has a positive, not a negative, effect on lipid balance.

Tyrosine phosphorylation of CEACAM1 by Src kinase in CEACAM1 KO and mutant cells

CEACAM1-LF is phosphorylated on ITIM Tyr488 (Tyr493 in man) by insulin receptor in murine hepatocytes treated with insulin (3). In contrast, human CEACAM1-LF is known to be phosphorylated on its ITIM tyrosines by Src kinases in lymphocytes (7). When WT HepG2 cells were treated ± insulin, CEACAM1 immunoprecipitated, and the IPs immunoblotted for phosphotyrosine, the results show maximal activity at 10 min, with sustained phosphorylation over 60 min (Fig. 8A). In contrast to CEACAM1 phosphorylation by insulin receptor in murine liver, maximal activity is within a few minutes (55). When the time course of phosphorylation was repeated on the mutant cell lines, the effect of added insulin was minimal on WT cells and accounted for <25% of the response for the S508A and S508D mutants (Fig. 8B). Notably, the tyrosine mutants, Y493F and Y520F, that had WT Y520 and Y493, respectively, had virtually undetectable levels of phosphotyrosine after insulin treatment (Fig. S3), demonstrating that insulin did not play a role in their phosphorylation. Based on these data, we investigated an alternate explanation for their phosphorylation.

Since Src was strongly expressed in the WT, KO, and mutant cells (Fig. S4), we hypothesized that Src, not insulin receptor, was responsible for the majority of tyrosine phosphorylation in CEACAM1-LF. The effect of Src inhibition, as well as PI-3K and CaMK2 inhibition, on the levels of phosphotyrosine in the S508A and S508D mutant lines was tested. As controls, CaMK2 inhibition was tested for its previous effect on phosphorylation of CEACAM1 (56) while PI-3K inhibition was tested based on its effect of CEACAM1 phosphorylation on the B-cell receptor (57). Almost complete inhibition of tyrosine-phosphorylation in CEACAM1 by a Src inhibitor but not by the PI-3K or CaMK2 inhibitors was observed (Fig. 8, *C* and *D*). In agreement with Src playing a major role in the tyrosine phosphorylation of both CEACAM1 and CD36, the two proteins colocalized in both PMs and BCs (Fig. 8, *E* and *F*). It is likely that CD36 may be associated with Src in hepatocytes, since CD36 is tyrosine-phosphorylated by Src kinases Fyn, Lyn, and Yes in platelets (36) and by Fyn in muscle (46), further connecting CEACAM1-LF and CD36 signaling.

CEACAM1, Src, LKB1, and annexin A2 co-IP with CD36 in the S508A mutant

Given the high expression of CD36 in the S508A mutant cells and its potential direct connection to CEACAM1-LF, as well as LKB1, Fyn, and AMPK that were found together in muscle (46), we immunoprecipitated CD36 and probed for CEACAM1, LKB1, Fyn, and AMPK, as well as Src, PCSK9, and Annexin A2. We

PCSK9 (green) Actin (red)   **CD36 (green)**   **PCSK9 (green)**
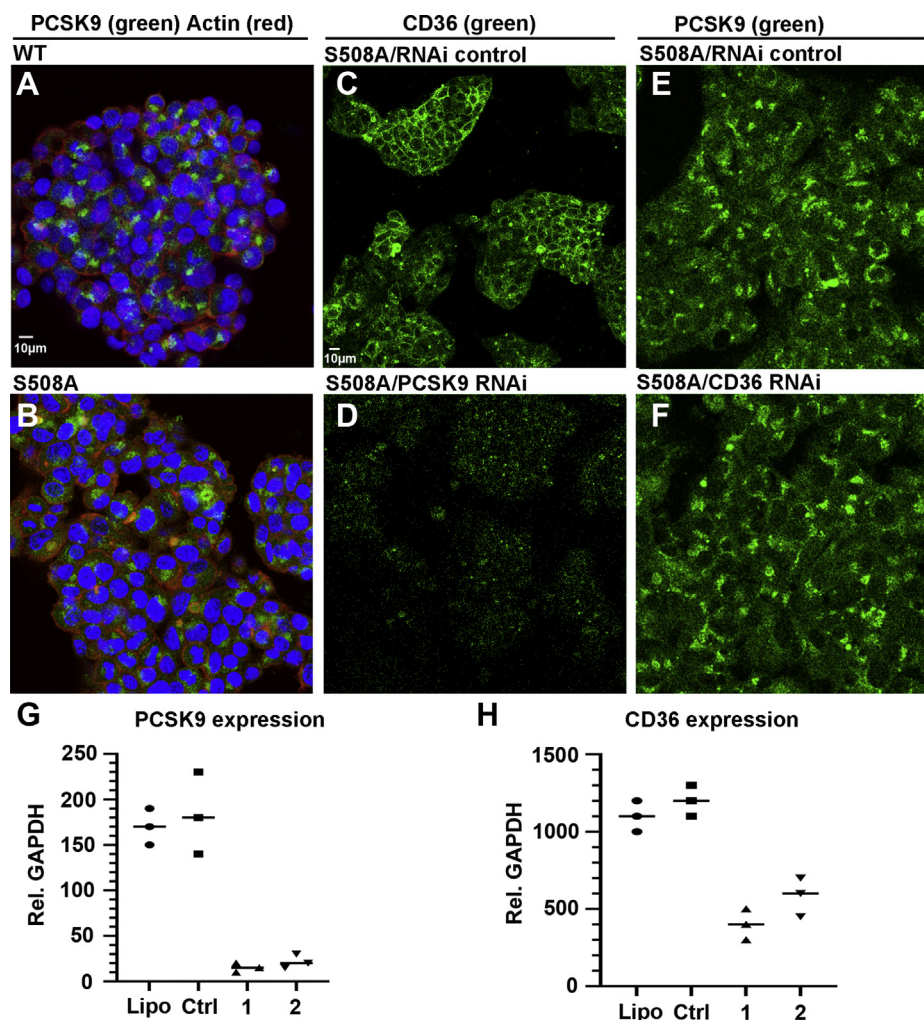
Figure 7. PCSK9 expression affects CD36 expression in the S508A mutant. PCSK9 expression in WT (*A*) and in CEACAM1 S508A mutant (*B*) HepG2 cells. Triple stained for PCSK9 (*green*), F-actin (*red*), and nuclei (*blue*). Effect of control RNAi (*C*) and PCSK9 RNAi (*D*) on CD36 expression (*green*) in CEACAM1 S508A mutant HepG2 cells. Lack of an effect of control RNAi (*E*) and CD36 RNAi (*F*) on PCSK9 expression (*green*). *G*, effect of PCSK9 RNAi on PCSK9 mRNA expression as measured by qRT-PCR. *H*, effect of PCSK9 RNAi on CD36 mRNA expression as measured by qRT-PCR in triplicate.

included Annexin A2 because of its role in Src-mediated endocytosis (58) and its previously shown association with CEACAM1 (11). The results show a strong association of CD36 with CEACAM1 and Src and weaker associations with LKB1 and Annexin A2 (Fig. 9). Blots for Fyn, AMPK, and PCSK9 were negative, although each was present in cell lysates (Fig. S5). It should be noted that the immunoblot for CEACAM1 in the CD36 IP resulted in the detection of bands at 130 and 85 kDa, the former corresponding to the expected molecular mass of CEACAM1-LF, and the latter to the molecular mass of BGP1 (4). Given the lower molecular mass of BGP1 *versus* CEA-CAM1, it is likely that BGP1 is a proteolytic fragment of CEACAM1. These results further confirm that CD36 associates with CEACAM1 and Src, while the absence of Fyn suggests that the CD36-Fyn association is restricted to muscle (46) and platelets (36), suggesting a cell-specific association of Src kinases. The association of LKB1 with CD36 is especially interesting in that loss of LKB1 in cultured hepatocytes impaired ABCB11 trafficking and BC formation (59), further linking CD36 and CEACAM1 to BC function.

SHP2 expression in CEACAM1 *KO* and mutant cells

Although tyrosine phosphorylation of CEACAM1 has been shown to recruit both SHP1 and SHP2 in epithelial cells (15), recruitment of SHP2 is preferred in hepatocytes and regulates IR endocytosis (17). When CEACAM1 was IPed from WT or CEACAM1 mutant HepG2 cell lines and the IPs blotted for SHP2 or SHP1, only SHP2 was detected (Fig. S6). Importantly, SHP2 recruitment did not depend on insulin, in contrast to the reported recruitment of SHP2 to tyrosine phosphorylated IRS1 and IRS2 (17). In addition, SHP2 was equally recruited to either the Y493F or Y502F mutants, indicating both tyrosines of CEACAM1 were phosphorylated by Src and served as substrates for SHP2. Thus, two distinct SHP2-mediated mechanisms are available for IR endocytosis, one mediated by insulin involving IRS1/2 (17), and one mediated by Src involving CEACAM1.

Comparative RNAseq analysis in CEACAM1 *KO* and mutant cells

RNAseq was performed to obtain a global readout of the gene expression of *CEACAM1*⁻/⁻ and the mutants S508A and
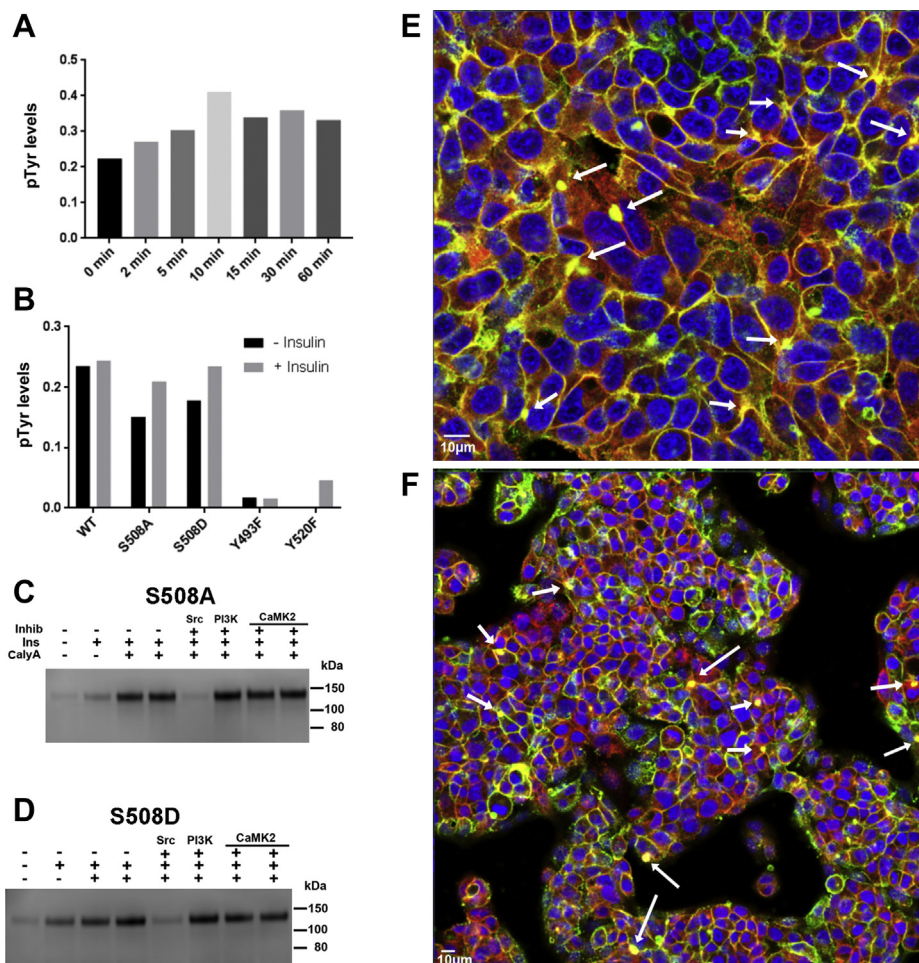
Figure 8. Tyrosine phosphorylation of CEACAM1 by insulin *versus* Src and coexpression of SRC and CD36 with CEACAM1 in mutant S508A cells. *A*, lysates (20 μg) from WT cells treated before and after with insulin (15 μg/ml) over time were IPed with anti-CEACAM1 antibody and immunoblotted for phosphotyrosine. *B*, lysates (20 μg) from cells treated before and after with insulin for 30 min were IPed with anti-CEACAM1 antibody and immunoblotted for phosphotyrosine (normalized for CEACAM1 signal in a parallel immunoblot). *C* and *D*, equal amounts of lysates from S508A (*C*) or S508D (*D*) mutants treated with insulin or inhibitors of Src (BOS, 10 μM), PI3K (LY294002, 20 μM), or CaMK2 (KN93, 20 μM), IPed with anti-CEACAM1 antibody and run on SDS gels were blotted for phosphotyrosine. Mutant S508A cells were stained for Src (*red*), CEACAM1 (*green*), DAPI (*blue*), and overlaid (*E*) or for Src (*red*), CD36 (*green*), DAPI (*blue*), and overlaid (*F*). *Arrows* indicate examples of prominent BCs with *yellow* staining indicating overlap of Src with CEACAM1 or CD36. Magnifications were 40× (*E*) and 20× (*F*).

S508D in HepG2 cells. Over 3000 protein coding genes were quantitated with the top upregulated genes for each cell line shown in Table S1. Since the upregulated genes are dominated by normal hepatocyte metabolism, a comparative analysis to WT was more informative (Fig. 10). The first of the top 50 upregulated S508A/WT genes is *AKNA*, encoding a microtubule organization and transcription factor regulated by a complex of PKA-CREB-NFκB, that is, in turn, is involved in inflammation (60). Since PKA is involved in phosphorylation of Ser512 in CEACAM1-LF (61), *AKNA* expression may provide a new link to the inflammatory phenotype of hepatosteatosis. The second gene, *ANO7* (anoctamin-7) is a phospholipid scramblase with a potential role in PI-3K-AKT-mTOR signaling (62), possibly connecting it to regulation of IR at the PM. The third, *DACT2* (dishevelled-associated antagonist of β-catenin) may indicate a further connection between CEACAM1 and β-catenin (63). Several of the PKA adaptor proteins (*AKAP6-8*) appear in the top ten, suggesting a role for PKA in the phosphorylation of CEACAM1-LF as

described in the companion paper. The 13th hit was *LPCAT3*, (lysophosphatidylcholine transferase-3), the enzyme that acylates lysophosphatidic acid with arachidonic acid (AA) and plays an important role in the secretion of TAGs (64). Since deletion of this gene in mice leads to hepatosteatosis (65), its expression is critical to maintain TAG homeostasis in the liver and may explain why it is upregulated in the S508A mutant. This finding prompted us to examine other genes regulating fatty acid metabolism in the RNAseq comparisons of the mutants to the WT cells. This led to the identification of high expression levels of Elongation of Very Long chain fatty acids (*ELOVL2*) and Fatty Acid Desaturase 1 and 2 (*FADS1* and *FADS2*), genes involved in the synthesis of 22:5 and 22:6 polyunsaturated FAs (Fig. S7, *A* and *B*). Notably, these FAs predominated in the upregulated TAGs of *CEACAM1⁻/⁻* cells (Table 2). The dramatic upregulation of the delta-6 desaturase gene FADS2 in the S508D mutant is especially interesting in that upregulation of this gene correlates with NAFLD (66). In addition, there was >200-fold increase in the expression of the
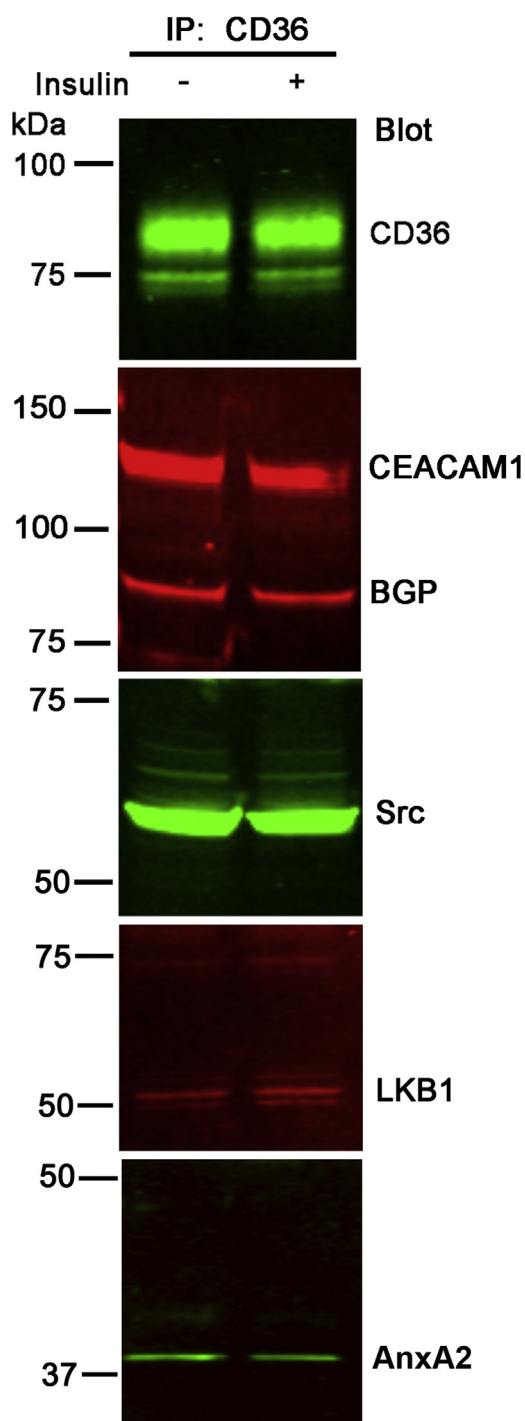
Figure 9. Coimmunoprecipitation of CEACAM1, Src, LB1, and Annexin A2 with CD36. CD36 was immunoprecipitated from Ser508A mutant HepG2 cells, pretreated or not with insulin, run on SDS gels, and immunoblotted for CD36, CEACAM1, Src, LKB1, and Annexin A2 (AnxA2). Equal amounts of protein were probed on immunoblots.

Abhydrolyase domain 6 gene (*ABHD6*) in the S508A/WT *versus* KO/WT (Fig. S7C). While ABHD5, also known as CGI-58, activates ATGL, the first step in TAG lipolysis, at the surface of lipid droplets (67), the related protein ABHD6 is a lipase that releases AA from monoacylglycerols (68), potentially connecting AA-TAGs and LPCAT3 to inflammation given the role of AA in PGE synthesis. AA, a 20:4 PUFA, is a

precursor to the above mentioned 22:5 and 22:6 PUFAs. The 29th hit in the S508A/WT RNAseq data was *CD36*, a major subject of interest in this study. The top hit for KO/WT was *AKT1S1* encoding PRAS40. PRAS40 plays a prominent role in insulin resistance since its phosphorylation by AKT1 (the second top hit), a downstream target of IR activation, leads to its association with mTORC1 (69). mTORC1, in turn can inhibit activation of AMPK (70), which is further connected to CD36 and FA binding (71). Since PPARγ, a major transcriptional regulator of CD36 (72), is not highly expressed in the liver compared with PPARα (73), we compared their expression in the six cell lines as analyzed by RNAseq (Fig. S8). Except for the WT cells, the levels of both PPARα and PPARγ were similar, suggesting that CD36 levels were mainly regulated by the degradation pathway. Overall, comparative RNAseq analysis provides further strength to the lipid storage connection between CEACAM1 and CD36 as probed by the CEACAM1 mutants.

Discussion

Although there is ample evidence for the association of CEACAM1 with obesity, NAFLD, and insulin resistance in the murine *Ceacam1* knockout model (74), including a potential functional role for Ser503 in the cytoplasmic domain (19), the evidence for analogous human CEACAM1 functional associations has not been established. As mentioned in the introduction and analyzed in the companion paper, the amino acid sequence around Ser508 (the human equivalent of rodent Ser503) suggests that the kinase specificity may differ between rodent and humans. If the kinase responsible for phosphorylation of Ser508 is not PKC in humans, then the regulatory pathway requires a thorough investigation. In choosing an appropriate human model for this study, we selected HepG2 cells that, like human hepatocytes, retain high expression of CEACAM1 and polarize to form BCs *in vitro*. The requirement for a BC model was evidenced in Figure 3, in which both the genetic knockdown of *CEACAM1* and the reintroduction of the Ser508 and Tyr493 and Tyr520 mutants into the genetically ablated cells caused changes, not only in the lipid droplet content, but also in their BC size. This relationship suggests the possibility that the steady-state levels of lipid droplets depend on BC function. Since it is well known that reverse cholesterol transport from the liver to intestine occurs through bile (75), and that BGP1 is a major cholesterol associated component of bile (4, 76), it would not be a surprise if hepatocytes also had the capacity to reverse transport other lipids into bile. Indeed, phospholipids constitute a major portion (10–20 mol percent) of bile (47). Since bile contains phospholipids and not free FAs, FAs would need to be transferred to lysophosphatidylcholine by an enzyme such as LPCAT3. In support of this possibility, LPCAT3 was the 13th top hit of S508A/WT upregulated genes determined by comparative RNAseq analysis (Fig. 10). Considering the volume of bile produce per day in the average human (400–800 ml) and with up to 20% content of phospholipids, the excretion of lipids back into the intestinal tract during
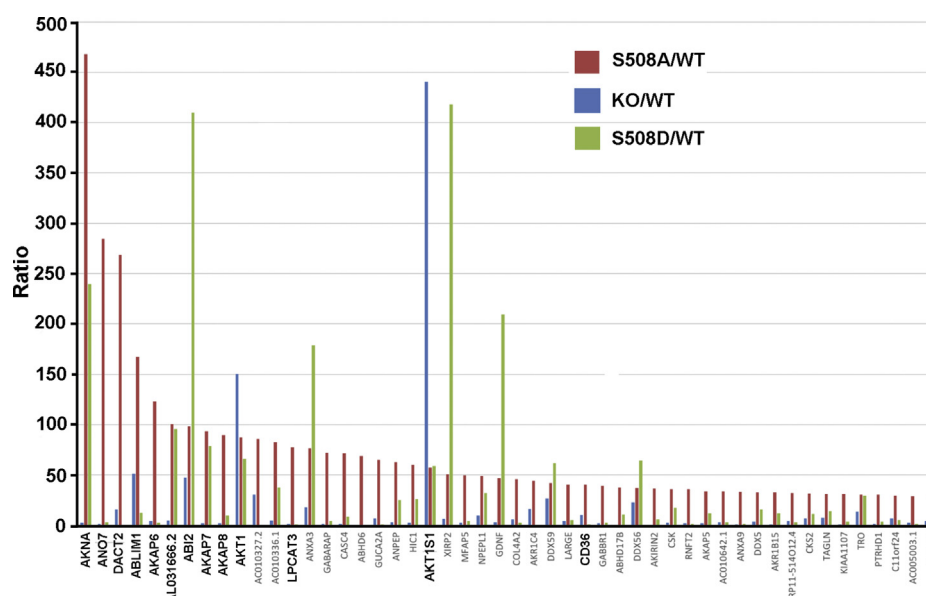
Figure 10. Comparative RNAseq analysis of WT *versus* CEACAM1$^{-/-}$, and S508A and S508D mutant cells. The ratio (cell line/WT) of the top 50 upregulated genes are shown with the first ten in *bold*, as well as additional hits discussed in the text.

feeding would help normalize the lipid content of the liver and delay systemic reabsorption. This possibility is currently under investigation by us.

The transport of FAs into hepatocytes is mediated by CD36 (35), which, like CEACAM1-LF, is associated with inflammation, especially in macrophages (39). We have established a close association between CEACAM1-LF and CD36, in that CD36 expression increases and associates with BCs in the S508A mutant line that has the least amount of lipid droplets and the largest BC size (Fig. 5) and that CEACAM1 and CD36 co-IP (Fig. 9). The fact that downregulation of CD36 with RNAi reverses the phenotype suggests cross talk between the signaling of CD36 and CEACAM1-LF, likely mediated by their similar association with a Src kinase (Fig. 8) and supported by the co-IP of Src with CD36 (Fig. 9). While previous studies showed that PCSK9 regulates the protein levels of CD36 in hepatocytes and that downregulation of PCSK9 resulted in elevated CD36 and lipid droplets in hepatocytes (44, 54), we now show that the lipid droplet levels can be lowered by high expression of CD36, especially in BCs, when CEACAM1-LF signaling is abrogated at the level of Ser508 (Fig. 7). We present a model that incorporates CEACAM1 regulation of FA import into hepatocytes by CD36 and subsequent lipid storage (Fig. 11, *A* and *B*). Depending on CEACAM1 signaling at the level of Ser508 and ITIM phosphorylation, the FA cargo would either be stored as TAGs accompanied with degradation of CD36 by PCSK9 (S508D and Y520F phenotypes) or shunted to BCs *via* CD36 translocation (S508A and Y493 phenotypes) where the FA cargo could be excreted, presumably as phospholipids.

The changes in lipid droplet accumulation observed in the comparative study of WT *versus* genetically abrogated *CEACAM1* and the mutant cell lines were further amplified in the comparative lipidomic study that showed an increase in unsaturated FAs. Strikingly, 22:5 and 22:6 PUFAs predominated in the upregulated TAGs of *CEACAM1*$^{-/-}$ cells (Table 2).

Docosapentaenoic acid (DPA 22:5) and docosahexaenoic acid (DHA 22:6) are important omega-6 and omega-3 PUFAs. DPA is derived from arachidonic acid by stepwise action of elongases and desaturases, of which both transcripts were upregulated in the comparative RNAseq analysis of the *CEACAM1* knockout cells (Fig. S7, *A* and *B*). The PUFA arachidonic acid is the precursor to the synthesis of prostaglandins, major mediators of inflammation. Thus, *CEACAM1*$^{-/-}$ cells exhibit a proinflammatory phenotype in terms of their upregulated lipid profile, while WT HepG2 cells have a lipid profile resembling normal liver (77). Since CEACAM1-LF encodes two ITIM receptors, CEACAM1-LF may play an important role in the suppression of inflammation in the liver, while its loss would result in an inflammatory phenotype. This may be a dual function of CEACAM1-LF, since its loss also leads to an increase in lipid droplet retention in which the lipid profile is upregulated in PUFAs. Furthermore, high expression levels of CEACAM1 in human donor livers correlate with successful liver transplantation (78).

Insulin resistance is highly correlated with the development of NAFLD (79). The cause of this correlation in humans is unknown. However, *Ceacam1* knockout mice exhibit both insulin resistance and NAFLD (74) and reconstitution of CEACAM1 liver expression in these mice reverses both phenotypes (80). The mechanism of insulin resistance in these mice has been largely ascribed to the portal clearance of insulin and subsequent internalization of IR by CEACAM1, but more recent studies have shown additional mechanisms. In the study by Choi *et al.* (17), the mechanism of IR internalization was regulated by SHP2 and MAPK, and the inhibition of SHP2 restored IR translocation to the PM, rendering the cells insulin responsive. In that study, SHP2 was found associated with IRS1/2, substrates of the IR. In our study, SHP2 also was recruited to CEACAM1-LF, suggesting a common mechanism for insulin clearance converging on SHP2 recruitment.
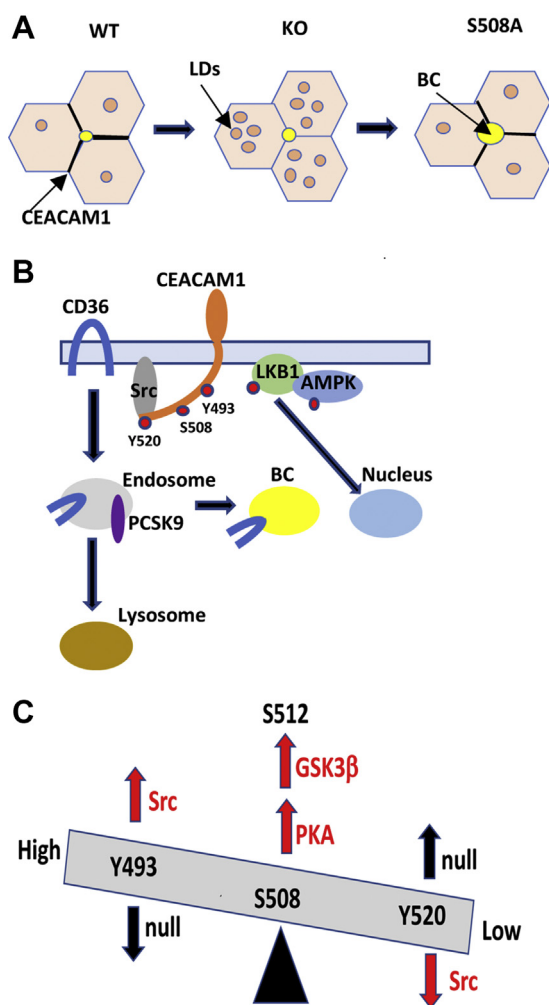
Figure 11. Model of FA import by CD36 and lipid droplet management in WT, CEACAM1$^{-/-}$, and CEACAM1 mutants in HepG2 cells. *A*, lipid droplets (LDs) increase in CEACAM1$^{-/-}$ *versus* WT cells and are reduced in S508A mutant cells along with an increase in size of bile canaliculi (BCs). *B*, CD36 is found in a complex with CEACAM1, Src, LKB1, and AMPK. Src can phosphorylate CEACAM1 on Y493 and Y520 located on either side of S508. LKB1 can phosphorylate AMPK; however, phosphorylated LKB1 can translocate to the nucleus, reducing phosphorylation of AMPK. CD36 can be internalized to endosomes after binding long chain fatty acids and shunted to either lysosomes for degradation or to BCs. *C*, phosphorylation of S512 by PKA followed by phosphorylation of S508 by GSK3β can lead to high lipid accumulation. Src phosphorylation of Y493 leads to high lipid accumulation, while phosphorylation of Y520 leads to low lipid accumulation. Phosphorylation of both tyrosines is influenced by the phosphorylation status of S508. Thus, the null mutants of Y493 and Y520 can abrogate their normal lipid regulation functions.

The role of SHP2 can also be explained, given the linkage between Ser508 and tyrosine phosphorylation: the S508A null mutation phenocopies the Y493F null mutant in which only Y520 can be phosphorylated, while the S508D phosphorylation mimic phenocopies the Y520F null phenotype in which only Y493 can be phosphorylated. Thus, it is possible that the phosphorylation status of S508 can determine the extent of phosphorylation and/or SHP2 recruitment to Y493 or Y520. Based on the kinetic studies performed on native *versus* PKA/GSK3β phosphorylated CEACAM1-LF cytoplasmic domain peptide in the companion paper, Src had a preference for Y520 over Y493 (not affected by S508 phosphorylation), and SHP2

had a preference for dephosphorylation (a surrogate for its recruitment to pTyr) that was affected by S508. Since both phosphotyrosines can recruit SHP2 (Fig. S6), the role of Ser508 may set the balance of recruitment of SHP2 between the two tyrosines: predominant pTyr-493 leads to increased lipid storage, and predominant pTyr-520 leads to decreased lipid storage (Fig. 11*C*). In WT cells, there is an obvious balance between the two, but in *CEACAM1$^{-/-}$* or in the Ser508D mutant cells, the balance is tipped toward lipid storage because of either the lack of CEACAM1-LF signaling or the pro-lipid storage signaling caused by the Ser508D mutation. This mechanism would allow the liver to adjust to conditions of high (feeding) *versus* low (fasting) lipid availability.

The requirement for Src kinase to phosphorylate the tyrosines of CEACAM1-LF is an important observation, for it not only links signaling between CD36 and CEACAM1, but also brings into play LKB1 and AMPK. In muscle, CD36 is found in a complex with Fyn, LKB1, and AMPK (46). Low levels of FAs result in the phosphorylation of LKB1 by Fyn and sequestration of LKB1 in the nucleus, while high levels of FAs cause dissociation of Fyn, promoting phosphorylation of AMPK by LKB1. The situation in the liver has not been studied. Our study suggests that nuclear LKB1 sequestration in hepatocytes is regulated by CEACAM1-LF, since the S508A mutant cells have about 45% of LKB1 sequestered in the nucleus, compared with 14% in the S508D mutant (Fig. 6, *A–D*). *CEACAM1$^{-/-}$* cells are almost completely unable to sequester LKB1 in the nucleus, implying a profound disturbance in this pathway. The result of loss of CEACAM1 expression is hyperactivation of AMPK (Fig. 6*F*), a compensatory response to hepatosteatosis (53). Thus, lipid storage/metabolic regulation in hepatocytes depends on the association of Src with both CEACAM1-LF and the CD36/LKB1/AMPK complex. We propose that the role of CEACAM1-LF is recruitment of Src to the complex, wherein the absence of CEACAM1-LF prevents this regulation.

For the regulatory mechanisms of human CEACAM1-LF to be fully understood, the kinases responsible for the phosphorylation of Ser-508 must be identified. As shown in the Introduction, there is a consensus sequence for GSK3β at Ser-508, including the required priming +4Ser at Ser512. We show in a companion paper that the cytoplasmic domain peptide of CEACAM1-LF was phosphorylated by GSK3β only when pretreated with PKA and not with CKI the priming kinase for glycogen synthase (26). Since many of the PKA adaptor proteins (AKAPs) were upregulated in the S508A mutant (Fig. 10), the activation and membrane attachment of PKA would bring it in close proximity to CEACAM1. Since PKA can inactivate GSK3β (81), continued PKA activation could limit the action of GSK3β on Ser508 of CEACAM1-LF. This yin-yang regulation is also observed for glucagon activation by PKA, in that PKA inactivates glycogen synthase (glucose storage in the liver) by inactivation of GSK3β. Thus, in WT CEACAM1-LF, PKA and GSK3β could act together to phosphorylate Ser508 (equivalent of S508D mutation) leading to lipid accumulation (Fig. 11*C*) until PKA inactivates GSK3β leading to reduction of lipid accumulation (equivalent to the S508A mutation). Since

GSK3β is inactivated by AKT during insulin signaling ([82]), GSK3β inactivation would prevent phosphorylation of Ser508 (equivalent to the S508A mutation) and reduce liver lipid storage. In the case of insulin resistance in the liver, lipid storage reduction would not occur, leading to hepatosteatosis ([Fig. 11*C*]). The complete loss of CEACAM1-LF in the liver would abrogate the fine control mechanism regulating lipid storage in the liver, as observed for *Ceacam1*$^{-/-}$ mice fed normal chow. There is also a potential role for β-catenin since its binding of CEACAM1-LF would lead to sequestration of CEACAM1 after phosphorylation of β-catenin with PKA. This interaction requires the action of PKA on both CEACAM1-LF and β-catenin (see companion paper). Sequestration of CEA-CAM1 would have a similar effect as the KO phenotype (lipid accumulation), but not as severe since the majority of CEA-CAM1 would be free. Since GSK3β phosphorylation of β-catenin can lead to its destruction ([83]), a further level of control may exist.

Conclusion

This study provides knockdown and mutation data showing human CEACAM1-LF regulates lipid storage and FA composition in human HepG2 cells. First: the CEACAM1 knockdown cells phenocopy the lipid accumulation seen in livers of *Ceacam1* knockdown mice. Second: mutational analysis of Ser508 or ITIM Ty493 or Tyr520 in the cytoplasmic domain of CEACAM1 identifies these residues as de-terminants of the lipid storage phenotype and correlates with the action of PKA/GSK3β and Src kinase on these residues. Third: CEACAM1, Src, and LKB1 co-IP with the fatty acid transporter CD36 that when knocked down with RNAi in-creases lipid droplet accumulation in CEACAM1 S508A mutant cells. Moreover, LKB1, an AMPK kinase regulated by CD36 and Src kinases, undergoes nuclear translocation correlated with CEACAM1 and CD36 phenotypes.

Experimental procedures

Materials

Vala Science's Lipid Staining reagent (4805) was from Vala Sciences; anti-SRC (ab231081), anti-CEACAM1 (ab108397), and anti-LKB1 (ab 15095) antibodies were from Abcam; Phalloidin Red (5783), DAPI (5748/10), and anti-CD36 anti-body (AF1955) were from R&D Systems. Alexa Fluor IgGs (B40192) were from Life Technologies. CD36 small interfering RNAs were from Life Technologies. HepG2 cells from ATCC were cultured in Earl's minimal essential medium (DMEM low glucose) +10% Fetal bovine serum, 2 mM GlutaMAX, 5 mM Glucose. RNA Easy and iScript cDNA Synthesis kits were from Qiagen and BioRad, respectively. Oligonucleotides were from Life Technologies or Qiagen ([Table S2], *A* and *B*). Confocal studies were performed on a Carl Zeiss confocal laser scanning microscope.

Generation of CEACAM1$^{-/-}$ and mutant cell lines

CEACAM1 was knocked out in HepG2 cells *via* CRISPR/Cas9 deletion as follows: guide RNAs targeting CEACAM1 were generated using the CRISPR web design tool (http://crispr.mit.edu) and inserted into pSpCas9(BB)-2A-Puro (PX459, Addgene plasmid # 62988), a gift from Dr Feng Zhang (Ran FA, Hsu PD, Wright J, Agarwala V, Scott DA, Zhang F. *Nat. Protoc.* 2013 Nov;8(11):2281-308). Ten sgRNAs were screened using the SURVEYOR nuclease Assay (Transgenomic 706020) and transfected into HepG2 cells with Lipofectamine 2000. The sgRNA that led to a successful CEACAM1$^{-/-}$ line was: 5′-CACGCCAATAACTCAGTCAC-3′. HepG2 CEACAM1$^{-/-}$ cells were enriched by puromycin selection and negatively sorted on a BD FACSAria Fusion cell sorter to produce a CEACAM1$^{-/-}$ cell line. Flow cytometry and immunoblot anal-ysis confirmed the loss of CEACAM1 expression. Mutants were generated by the Agilent site directed mutageneis kit and transfected into the CEACAM1$^{-/-}$ cell line.

Lipidomics

Sample preparation and analysis were performed as previ-ously described ([84]). Briefly, frozen cell pellets (1 million cells) were suspended in 500 μl PBS containing 200 μM EDTA and 10 μM t-butylated hydroxytoluene (BHT), extracted with 1.5 ml chloroform methanol (2:1), concentrated and dissolved in 100 μl 10% acetonitrile in isopropanol containing 10 mM ammonium formate, separated by UHPLC at 300 μl/min in a Phenomenex Kinetex C18 2.1 × 100 mm, 100A, 1.7 μm maintained at 55 °C with gradient elution, and analyzed on a Thermo Orbitrap Lumos. The data was analyzed by Thermo Lipid Search v4.2. Only lipids with a *p* value <0.05 and an identification score of A or B were selected in the final results. The peak area of all lipids was normalized to POPC, the most intense lipid in HepG2 cells. The data for each cell line was reported as ratios to WT cells ([Table 2]). A complete analysis of all lipids in the cell lines is available upon request.

Lipid staining of cell lines

HepG2 cells 3 × 10^5 cells per well were plated on 4-well glass chamber slides for 24 to 72 h, fixed, and permeablized with 4% paraformaldehyde in PBS and Vala Science's Lipid Staining reagent added in blocking buffer (10% normal goat serum, 3% bovine serum albumin, 0.02% sodium azide, in PBS) for 30 min to label neutral lipids in the green fluorescence channel. The samples were then rinsed three times with PBS and stained for nuclei by incubating for 20 min in DAPI (250 ng/ml in 10 mM Tris, 10 mM EDTA, 100 mM NaCl, 0.02% sodium azide, buffered to pH 7.4). LDs, divided into large (≥1 μm) or small (<1 μm) were counted from three fields of 50 cells, the mean values and SEMs determined, then *p* values *versus* WT calculated by analysis of variance by one way ANOVA with a post hoc confidence interval of 95.

Kinase inhibitor treatments

Cells were plated on 60-mm dishes at a density of 1 × 10^6 cells per dish over three nights to reach confluency in DMEM-low glucose supplemented with 10% FBS, 1× Antibiotic-Antimycotic, and 1 mM sodium pyruvate. Cells were serum starved overnight in medium MEM. Cell culture media

was changed to fresh MEM and 0.1% DMSO. Cells were either pretreated with or without final concentration of 10 μM of kinase inhibitors in 0.1% DMSO for 30 min prior to adding 15 μg/ml of insulin. Media was removed and cells washed with PBS following lysis of cells for immunoprecipitation of CEACAM1.

Immunoprecipitation and immunoblot analysis

CEACAM1 IPs: Cells (10^6) were serum starved overnight, ± insulin treatment (15 μg/ml) for 10 min, lysed at $4\,°C$ with IP lysis buffer (Thermo Scientific) containing sodium orthovanadate, calyculin A, and protease inhibitors. Equal protein amounts of lysates (BCA assay, Themo Scientific) were precleared with 50 μg mIgG prebound to 50 μl Protein A/G plus agarose bead slurry (Thermo Scientific) for 30 min, added to 50 μg anti-CEACAM1 T84.1 (49) prebound to 50 μl Protein A/G plus agarose bead slurry, and incubated overnight at $4\,°C$. After washing three times with 500 μl IP lysis buffer, samples were eluted with 50 μl of 2× SDS sample buffer, and equal protein amounts (BCA assay, Thermo Scientific) separated on SDS-PAGE gels and transferred onto PVDF membranes (Invitrogen, IB401001) using iBlot Transfer Stack with the iBlot Dry Blotting System. Blots stained with ECL reagent were blocked with 5% BSA in TBS and blots stained with LI-COR reagents were blocked with Intercept Blocking Buffer (LI-COR, 927-60001) for 1 h at room temperature on a shaker. LI-COR blots were stained with primary antibody in Intercept T20 (TBS) Antibody Diluent (LI-COR, 927-65001) overnight at $4\,°C$ on a shaker and probed with anti-phosphotyrosine 4G10 Platinum HRP conjugate (Millipore Sigma) or anti-CEACAM1 antibody T84.1. CD36 IPs: Cells (10^6) were serum starved, treated ± insulin as above, lysed with 1 ml of Ultra RIPA A (DiagnoCine, F015), and precleared as above. Goat anti-human CD36 (50 μg; R&D, AF1955) was immobilized on a Thermo Scientific IP column, 26149, washed 3× with lysis buffer, incubated with cell lysates, washed 3× with lysate buffer, and eluted with 2× SDS sample buffer. SDS gel electrophoresis and transfer to PVDF membranes were performed as above. Blots were immunostained with goat anti-human CD36 (R&D, AF1955), mouse anti-human CEACAM1 (T84.1), rabbit anti-human Src (Abcam, AB109381), mouse anti-human LKB1 (Invitrogen, AH01392), mouse anti-human 4G10 (Sigma-Aldrich, 05-321), goat anti-human Annexin A2 (R&D, AF3928-SP), rabbit anti-human phospho-Src (R&D, MAB2685), rabbit β-Catenin (Abcam, Ab32572), rabbit anti-human PCSK9 (Invitrogen, AH01392), mouse anti-human AMPKα (Invitrogen, AH01332), or mouse anti-human FYN (Invitrogen, MA1-19331). Secondary antibodies were IRDye 800CW Donkey anti-Goat IgG Secondary Antibody (LI-COR, 926-32214), IRDye 800CW Goat anti-Rabbit IgG Secondary Antibody (LI-COR, 926-32211), or IRDye 680RD Goat anti-Mouse IgG Secondary Antibody (LI-COR, 926-68070).

Confocal studies

Cells (3×10^5 cells per well) were plated on 4-well glass chambers (Thermo Scientific) for 24 to 72 h. Basic culture medium was removed, cells were washed with PBS, fixed with 4% paraformaldehyde in PBS for 30 min, and permeabilized with NP40 containing 0.01% saponin for 15 min. The cells were washed with PBS and stained with anti CEACAM1 antibody (mouse monoclonal antibody N-1(Santa Cruz), phalloidin red and DAPI), and visualized on a Carl Zeiss confocal laser scanning microscope.

Data availability

The raw data for these studies are available from the senior author at jshively@coh.org.

Author contributions—J. E. S. conceptualization; J. C., C.-J. C., G. G., P. W., S. C., H. L., and T. N. data curation; G. G. and S. B. formal analysis; J. C., C.-J. C., G. G., P. W., S. C., H. L., T. N., S. B., and J. E. S. investigation; J. E. S. resources; J. E. S. supervision; J. E. S. writing —original draft; J. C., C.-J. C., G. G., and J. E. S. writing—review and editing.

Abbreviations—The abbreviations used are: BC, bile canaliculi; CEACAM1, carcinoembryonic antigen-related cell adhesion molecule-1; FA, fatty acid; GSK3β, glycogen synthase kinase-3β; ITIM, immunoreceptor tyrosine inhibitory motif; LKB1, liver kinase B-1; NAFLD, nonalcoholic fatty liver disease; PCSK9, proprotein convertase subtilisin/kexin type 9 serine protease; SHP1/2, src homology domain protein phosphatase-1/2; TAG, triacylglyceride; VLDL, very low density lipid.

References

1. Svenberg, T., Hammarstrom, S., and Zeromski, J. (1979) Immunofluorescence studies on the occurrence and localization of the CEA-related biliary glycoprotein I (BGP I) in normal human gastrointestinal tissues. *Clin. Exp. Immunol.* **36**, 436–441
2. Beauchemin, N., Draber, P., Dveksler, G., Gold, P., Gray-Owen, S., Grunert, F., Hammarstrom, S., Holmes, K. V., Karlsson, A., Kuroki, M., Lin, S. H., Lucka, L., Najjar, S. M., Neumaier, M., Obrink, B., *et al.* (1999) Redefined nomenclature for members of the carcinoembryonic antigen family. *Exp. Cell Res.* **252**, 243–249
3. Poy, M. N., Yang, Y., Rezaei, K., Fernstrom, M. A., Lee, A. D., Kido, Y., Erickson, S. K., and Najjar, S. M. (2002) CEACAM1 regulates insulin clearance in liver. *Nat. Genet.* **30**, 270–276
4. Jirsa, M., Muchova, L., Draberova, L., Draber, P., Smid, F., Kuroki, M., Marecek, Z., and Groen, A. K. (2001) Carcinoembryonic antigen-related cell adhesion molecule 1 is the 85-kilodalton pronase-resistant biliary glycoprotein in the cholesterol crystallization promoting low density protein-lipid complex. *Hepatology* **34**, 1075–1082
5. Kitamura, Y., Murata, Y., Park, J. H., Kotani, T., Imada, S., Saito, Y., Okazawa, H., Azuma, T., and Matozaki, T. (2015) Regulation by gut commensal bacteria of carcinoembryonic antigen-related cell adhesion molecule expression in the intestinal epithelium. *Genes Cells* **20**, 578–589
6. Tchoupa, A. K., Schuhmacher, T., and Hauck, C. R. (2014) Signaling by epithelial members of the CEACAM family - mucosal docking sites for pathogenic bacteria. *Cell Commun. Signal.* **12**, 27

7. Gray-Owen, S. D., and Blumberg, R. S. (2006) CEACAM1: Contact-dependent control of immunity. *Nat. Rev. Immunol.* **6**, 433–446

8. Kilic, N., Oliveira-Ferrer, L., Wurmbach, J. H., Loges, S., Chalajour, F., Neshat-Vahid, S., Weil, J., Fernando, M., and Ergun, S. (2005) Pro-angiogenic signaling by the endothelial presence of CEACAM1. *J. Biol. Chem.* **280**, 2361–2369

9. Schumann, D., Chen, C. J., Kaplan, B., and Shively, J. E. (2001) Carcinoembryonic antigen cell adhesion molecule 1 directly associates with cytoskeleton proteins actin and tropomyosin. *J. Biol. Chem.* **276**, 47421–47433

10. Sadekova, S., Lamarche-Vane, N., Li, X., and Beauchemin, N. (2000) The CEACAM1-L glycoprotein associates with the actin cytoskeleton and localizes to cell-cell contact through activation of Rho-like GTPases. *Mol. Biol. Cell* **11**, 65–77

11. Kirshner, J., Schumann, D., and Shively, J. E. (2003) CEACAM1, a cell-cell adhesion molecule, directly associates with annexin II in a three-dimensional model of mammary morphogenesis. *J. Biol. Chem.* **278**, 50338–50345

12. Hu, W., Bhattacharya, S., Hong, T., Wong, P., Li, L., Vaidehi, N., Kalkum, M., and Shively, J. E. (2021) Structural characterization of a dimeric complex between the short cytoplasmic domain of CEACAM1 and the pseudo tetramer of S100A10-annexin A2 using NMR and molecular dynamics. *Biochim. Biophys. Acta Biomembr.* **1863**, 183451

13. Billadeau, D. D., and Leibson, P. J. (2002) ITAMs versus ITIMs: Striking a balance during cell regulation. *J. Clin. Invest.* **109**, 161–168

14. Brummer, J., Neumaier, M., Gopfert, C., and Wagener, C. (1995) Association of pp60c-src with biliary glycoprotein (CD66a), an adhesion molecule of the carcinoembryonic antigen family downregulated in colorectal carcinomas. *Oncogene* **11**, 1649–1655

15. Huber, M., Izzi, L., Grondin, P., Houde, C., Kunath, T., Veillette, A., and Beauchemin, N. (1999) The carboxyl-terminal region of biliary glycoprotein controls its tyrosine phosphorylation and association with protein-tyrosine phosphatases SHP-1 and SHP-2 in epithelial cells. *J. Biol. Chem.* **274**, 335–344

16. Beauchemin, N., Kunath, T., Robitaille, J., Chow, B., Turbide, C., Daniels, E., and Veillette, A. (1997) Association of biliary glycoprotein with protein tyrosine phosphatase SHP-1 in malignant colon epithelial cells. *Oncogene* **14**, 783–790

17. Choi, E., Kikuchi, S., Gao, H., Brodzik, K., Nassour, I., Yopp, A., Singal, A. G., Zhu, H., and Yu, H. (2019) Mitotic regulators and the SHP2-MAPK pathway promote IR endocytosis and feedback regulation of insulin signaling. *Nat. Commun.* **10**, 1473

18. Leung, N., Turbide, C., Olson, M., Marcus, V., Jothy, S., and Beauchemin, N. (2006) Deletion of the carcinoembryonic antigen-related cell adhesion molecule 1 (Ceacam1) gene contributes to colon tumor progression in a murine model of carcinogenesis. *Oncogene* **25**, 5527–5536

19. Lee, S. J., Heinrich, G., Fedorova, L., Al-Share, Q. Y., Ledford, K. J., Fernstrom, M. A., McInerney, M. F., Erickson, S. K., Gatto-Weis, C., and Najjar, S. M. (2008) Development of nonalcoholic steatohepatitis in insulin-resistant liver-specific S503A carcinoembryonic antigen-related cell adhesion molecule 1 mutant mice. *Gastroenterology* **135**, 2084–2095

20. Ghosh, S., Kaw, M., Patel, P. R., Ledford, K. J., Bowman, T. A., McInerney, M. F., Erickson, S. K., Bourey, R. E., and Najjar, S. M. (2010) Mice with null mutation of Ceacam I develop nonalcoholic steatohepatitis. *Hepat. Med.* **2010**, 69–78

21. Sippel, C. J., Fallon, R. J., and Perlmutter, D. H. (1994) Bile acid efflux mediated by the rat liver canalicular bile acid transport/ecto-ATPase protein requires serine 503 phosphorylation and is regulated by tyrosine 488 phosphorylation. *J. Biol. Chem.* **269**, 19539–19545

22. Dawson, P. A., Lan, T., and Rao, A. (2009) Bile acid transporters. *J. Lipid Res.* **50**, 2340–2357

23. Sippel, C. J., McCollum, M. J., and Perlmutter, D. H. (1994) Bile acid transport by the rat liver canalicular bile acid transport/ecto-ATPase protein is dependent on ATP but not on its own ecto-ATPase activity. *J. Biol. Chem.* **269**, 2820–2826

24. Bigonnesse, F., Levesque, S. A., Kukulski, F., Lecka, J., Robson, S. C., Fernandes, M. J., and Sevigny, J. (2004) Cloning and characterization of mouse nucleoside triphosphate diphosphohydrolase-8. *Biochemistry* **43**, 5511–5519

25. Rust, H. L., and Thompson, P. R. (2011) Kinase consensus sequences: A breeding ground for crosstalk. *ACS Chem. Biol.* **6**, 881–892

26. Sutherland, C. (2011) What are the bona fide GSK3 substrates? *Int. J. Alzheimers Dis.* **2011**, 505607

27. Frame, S., Cohen, P., and Biondi, R. M. (2001) A common phosphate binding site explains the unique substrate specificity of GSK3 and its inactivation by phosphorylation. *Mol. Cell* **7**, 1321–1327

28. Kammerer, R., and Zimmermann, W. (2010) Coevolution of activating and inhibitory receptors within mammalian carcinoembryonic antigen families. *BMC Biol.* **8**, 12

29. Laber, S., and Cox, R. D. (2017) Mouse models of human GWAS hits for obesity and diabetes in the post genomic era: Time for reevaluation. *Front. Endocrinol. (Lausanne)* **8**, 11

30. Su, R. C., Lad, A., Breidenbach, J. D., Blomquist, T. M., Gunning, W. T., Dube, P., Kleinhenz, A. L., Malhotra, D., Haller, S. T., and Kennedy, D. J. (2019) Hyperglycemia induces key genetic and phenotypic changes in human liver epithelial HepG2 cells which parallel the Leprdb/J mouse model of non-alcoholic fatty liver disease (NAFLD). *PLoS One* **14**, e0225604

31. Kiriyama, S., Yokoyama, S., Ueno, M., Hayami, S., Ieda, J., Yamamoto, N., Yamaguchi, S., Mitani, Y., Nakamura, Y., Tani, M., Mishra, L., Shively, J. E., and Yamaue, H. (2014) CEACAM1 long cytoplasmic domain isoform is associated with invasion and recurrence of hepatocellular carcinoma. *Ann. Surg. Oncol.* **21 Suppl 4**, S505–S514

32. Hokari, M., Matsuda, Y., Wakai, T., Shirai, Y., Sato, M., Tsuchiya, A., Takamura, M., Yamagiwa, S., Suzuki, K., Ohkoshi, S., Ichida, T., Kawachi, H., and Aoyagi, Y. (2007) Tumor suppressor carcinoembryonic antigen-related cell adhesion molecule 1 potentates the anchorage-independent growth of human hepatoma HepG2 cells. *Life Sci.* **81**, 336–345

33. Sormunen, R., Eskelinen, S., and Lehto, V. P. (1993) Bile canaliculus formation in cultured HEPG2 cells. *Lab. Invest.* **68**, 652–662

34. Olivecrona, G. (2016) Role of lipoprotein lipase in lipid metabolism. *Curr. Opin. Lipidol.* **27**, 233–241

35. Pepino, M. Y., Kuda, O., Samovski, D., and Abumrad, N. A. (2014) Structure-function of CD36 and importance of fatty acid signal transduction in fat metabolism. *Annu. Rev. Nutr.* **34**, 281–303

36. Huang, M. M., Bolen, J. B., Barnwell, J. W., Shattil, S. J., and Brugge, J. S. (1991) Membrane glycoprotein IV (CD36) is physically associated with the Fyn, Lyn, and Yes protein-tyrosine kinases in human platelets. *Proc. Natl. Acad. Sci. U. S. A.* **88**, 7844–7848

37. Chabowski, A., Gorski, J., Luiken, J. J., Glatz, J. F., and Bonen, A. (2007) Evidence for concerted action of FAT/CD36 and FABPpm to increase fatty acid transport across the plasma membrane. *Prostaglandins Leukot. Essent. Fatty Acids* **77**, 345–353

38. Miquilena-Colina, M. E., Lima-Cabello, E., Sanchez-Campos, S., Garcia-Mediavilla, M. V., Fernandez-Bermejo, M., Lozano-Rodriguez, T., Vargas-Castrillon, J., Buque, X., Ochoa, B., Aspichueta, P., Gonzalez-Gallego, J., and Garcia-Monzon, C. (2011) Hepatic fatty acid translocase CD36 upregulation is associated with insulin resistance, hyperinsulinaemia and increased steatosis in non-alcoholic steatohepatitis and chronic hepatitis C. *Gut* **60**, 1394–1402

39. Silverstein, R. L., and Febbraio, M. (2009) CD36, a scavenger receptor involved in immunity, metabolism, angiogenesis, and behavior. *Sci. Signal.* **2**, re3

40. Wilson, C. G., Tran, J. L., Erion, D. M., Vera, N. B., Febbraio, M., and Weiss, E. J. (2016) Hepatocyte-specific disruption of CD36 attenuates fatty liver and improves insulin sensitivity in HFD-fed mice. *Endocrinology* **157**, 570–585

41. Heinrich, G., Muturi, H. T., Rezaei, K., Al-Share, Q. Y., DeAngelis, A. M., Bowman, T. A., Ghadieh, H. E., Ghanem, S. S., Zhang, D., Garofalo, R. S., Yin, L., and Najjar, S. M. (2017) Reduced hepatic carcinoembryonic antigen-related cell adhesion molecule 1 level in obesity. *Front. Endocrinol. (Lausanne)* **8**, 54

42. Love-Gregory, L., and Abumrad, N. A. (2011) CD36 genetics and the metabolic complications of obesity. *Curr. Opin. Clin. Nutr. Metab. Care* **14**, 527–534

43. Shibao, C. A., Celedonio, J. E., Tamboli, R., Sidani, R., Love-Gregory, L., Pietka, T., Xiong, Y., Wei, Y., Abumrad, N. N., Abumrad, N. A., and Flynn, C. R. (2018) CD36 modulates fasting and preabsorptive hormone and bile acid levels. *J. Clin. Endocrinol. Metab.* **103**, 1856–1866

44. Demers, A., Samami, S., Lauzier, B., Des Rosiers, C., Ngo Sock, E. T., Ong, H., and Mayer, G. (2015) PCSK9 induces CD36 degradation and affects long-chain fatty acid uptake and triglyceride metabolism in adipocytes and in mouse liver. *Arterioscler. Thromb. Vasc. Biol.* **35**, 2517–2525

45. Lagace, T. A. (2014) PCSK9 and LDLR degradation: Regulatory mechanisms in circulation and in cells. *Curr. Opin. Lipidol.* **25**, 387–393

46. Samovski, D., Sun, J., Pietka, T., Gross, R. W., Eckel, R. H., Su, X., Stahl, P. D., and Abumrad, N. A. (2015) Regulation of AMPK activation by CD36 links fatty acid uptake to beta-oxidation. *Diabetes* **64**, 353–359

47. Muraca, M., Vilei, M. T., Miconi, L., Petrin, P., Antoniutti, M., and Pedrazzoli, S. (1991) A simple method for the determination of lipid composition of human bile. *J. Lipid Res.* **32**, 371–374

48. Horst, A. K., Najjar, S. M., Wagener, C., and Tiegs, G. (2018) CEACAM1 in liver injury, metabolic and immune regulation. *Int. J. Mol. Sci.* **19**, 3110

49. Chen, C. J., Kirshner, J., Sherman, M. A., Hu, W., Nguyen, T., and Shively, J. E. (2007) Mutation analysis of the short cytoplasmic domain of the cell-cell adhesion molecule CEACAM1 identifies residues that orchestrate actin binding and lumen formation. *J. Biol. Chem.* **282**, 5749–5760

50. Yokoyama, S., Chen, C. J., Nguyen, T., and Shively, J. E. (2007) Role of CEACAM1 isoforms in an *in vivo* model of mammary morphogenesis: Mutational analysis of the cytoplasmic domain of CEACAM1-4S reveals key residues involved in lumen formation. *Oncogene* **26**, 7637–7646

51. Najjar, S. M., Choice, C. V., Soni, P., Whitman, C. M., and Poy, M. N. (1998) Effect of pp120 on receptor-mediated insulin endocytosis is regulated by the juxtamembrane domain of the insulin receptor. *J. Biol. Chem.* **273**, 12923–12928

52. Yamada, E., Lee, T. W., Pessin, J. E., and Bastie, C. C. (2010) Targeted therapies of the LKB1/AMPK pathway for the treatment of insulin resistance. *Future Med. Chem.* **2**, 1785–1796

53. Smith, B. K., Marcinko, K., Desjardins, E. M., Lally, J. S., Ford, R. J., and Steinberg, G. R. (2016) Treatment of nonalcoholic fatty liver disease: Role of AMPK. *Am. J. Physiol. Endocrinol. Metab.* **311**, E730–E740

54. Lebeau, P. F., Byun, J. H., Platko, K., Al-Hashimi, A. A., Lhotak, S., MacDonald, M. E., Mejia-Benitez, A., Prat, A., Igdoura, S. A., Trigatti, B., Maclean, K. N., Seidah, N. G., and Austin, R. C. (2019) Pcsk9 knockout exacerbates diet-induced non-alcoholic steatohepatitis, fibrosis and liver injury in mice. *JHEP Rep.* **1**, 418–429

55. Najjar, S. M. (2002) Regulation of insulin action by CEACAM1. *Trends Endocrinol. Metab.* **13**, 240–245

56. Nguyen, T., Chen, C. J., and Shively, J. E. (2014) Phosphorylation of CEACAM1 molecule by calmodulin kinase IID in a three-dimensional model of mammary gland lumen formation. *J. Biol. Chem.* **289**, 2934–2945

57. Lobo, E. O., Zhang, Z., and Shively, J. E. (2009) Pivotal advance: CEACAM1 is a negative coreceptor for the B cell receptor and promotes CD19-mediated adhesion of B cells in a PI3K-dependent manner. *J. Leukoc. Biol.* **86**, 205–218

58. Valapala, M., and Vishwanatha, J. K. (2011) Lipid raft endocytosis and exosomal transport facilitate extracellular trafficking of annexin A2. *J. Biol. Chem.* **286**, 30911–30925

59. Porat-Shliom, N., Tietgens, A. J., Van Itallie, C. M., Vitale-Cross, L., Jarnik, M., Harding, O. J., Anderson, J. M., Gutkind, J. S., Weigert, R., and Arias, I. M. (2016) Liver kinase B1 regulates hepatocellular tight junction distribution and function *in vivo*. *Hepatology* **64**, 1317–1329

60. Liu, X., Huang, D., Guo, P., Wu, Q., Dai, M., Cheng, G., Hao, H., Xie, S., Yuan, Z., and Wang, X. (2017) PKA/CREB and NF-kappaB pathway regulates AKNA transcription: A novel insight into T-2 toxin-induced inflammation and GH deficiency in GH3 cells. *Toxicology* **392**, 81–95

61. Hu, W, Bagramyan, K, Bhatticharya, S, Hong, T, Tapia, A, Wong, P, Kalkum, M, and Shively, JE (2021) Phosphorylation of human CEACAM1-LF by PKA and GSK3β promotes its interaction with β-catenin. *J. Biol. Chem.* **297**, 101305

62. Lee, B. C., Khelashvili, G., Falzone, M., Menon, A. K., Weinstein, H., and Accardi, A. (2018) Gating mechanism of the extracellular entry to the lipid pathway in a TMEM16 scramblase. *Nat. Commun.* **9**, 3251

63. Li, J., Zhang, M., He, T., Li, H., Cao, T., Zheng, L., and Guo, M. (2017) Methylation of DACT2 promotes breast cancer development by activating Wnt signaling. *Sci. Rep.* **7**, 3325

64. Rong, X., Wang, B., Dunham, M. M., Hedde, P. N., Wong, J. S., Gratton, E., Young, S. G., Ford, D. A., and Tontonoz, P. (2015) Lpcat3-dependent production of arachidonoyl phospholipids is a key determinant of triglyceride secretion. *Elife* **4**, e06557

65. Cash, J. G., and Hui, D. Y. (2016) Liver-specific overexpression of LPCAT3 reduces postprandial hyperglycemia and improves lipoprotein metabolic profile in mice. *Nutr. Diabetes* **6**, e206

66. Walle, P., Takkunen, M., Mannisto, V., Vaittinen, M., Lankinen, M., Karja, V., Kakela, P., Agren, J., Tiainen, M., Schwab, U., Kuusisto, J., Laakso, M., and Pihlajamaki, J. (2016) Fatty acid metabolism is altered in non-alcoholic steatohepatitis independent of obesity. *Metabolism* **65**, 655–666

67. Sanders, M. A., Zhang, H., Mladenovic, L., Tseng, Y. Y., and Granneman, J. G. (2017) Molecular basis of ABHD5 lipolysis activation. *Sci. Rep.* **7**, 42589

68. Poursharifi, P., Madiraju, S. R. M., and Prentki, M. (2017) Monoacylglycerol signalling and ABHD6 in health and disease. *Diabetes Obes. Metab.* **19 Suppl 1**, 76–89

69. He, C. L., Bian, Y. Y., Xue, Y., Liu, Z. X., Zhou, K. Q., Yao, C. F., Lin, Y., Zou, H. F., Luo, F. X., Qu, Y. Y., Zhao, J. Y., Ye, M. L., Zhao, S. M., and Xu, W. (2016) Pyruvate kinase M2 activates mTORC1 by phosphorylating AKT1S1. *Sci. Rep.* **6**, 21524

70. Ling, N. X. Y., Kaczmarek, A., Hoque, A., Davie, E., Ngoei, K. R. W., Morrison, K. R., Smiles, W. J., Forte, G. M., Wang, T., Lie, S., Dite, T. A., Langendorf, C. G., Scott, J. W., Oakhill, J. S., and Petersen, J. (2020) mTORC1 directly inhibits AMPK to promote cell proliferation under nutrient stress. *Nat. Metab.* **2**, 41–49

71. Wiza, C., Nascimento, E. B., and Ouwens, D. M. (2012) Role of PRAS40 in Akt and mTOR signaling in health and disease. *Am. J. Physiol. Endocrinol. Metab.* **302**, E1453–1460

72. Marechal, L., Laviolette, M., Rodrigue-Way, A., Sow, B., Brochu, M., Caron, V., and Tremblay, A. (2018) The CD36-PPARgamma pathway in metabolic disorders. *Int. J. Mol. Sci.* **19**, 1529

73. Wang, Y., Nakajima, T., Gonzalez, F. J., and Tanaka, N. (2020) PPARs as metabolic regulators in the liver: Lessons from liver-specific PPAR-null mice. *Int. J. Mol. Sci.* **21**, 2061

74. Najjar, S. M., and Russo, L. (2014) CEACAM1 loss links inflammation to insulin resistance in obesity and non-alcoholic steatohepatitis (NASH). *Semin. Immunopathol.* **36**, 55–71

75. Gillard, B. K., Rosales, C., Xu, B., Gotto, A. M., Jr., and Pownall, H. J. (2018) Rethinking reverse cholesterol transport and dysfunctional high-density lipoproteins. *J. Clin. Lipidol.* **12**, 849–856

76. Svenberg, T., Hammarstrom, S., and Hedin, A. (1979) Purification and properties of biliary glycoprotein I (BGP I). Immunochemical relationship to carcinoembryonic antigen. *Mol. Immunol.* **16**, 245–252

77. Kotronen, A., Seppanen-Laakso, T., Westerbacka, J., Kiviluoto, T., Arola, J., Ruskeepaa, A. L., Yki-Jarvinen, H., and Oresic, M. (2010) Comparison of lipid and fatty acid composition of the liver, subcutaneous and intra-abdominal adipose tissue, and serum. *Obesity (Silver Spring)* **18**, 937–944

78. Nakamura, K., Kageyama, S., Kaldas, F. M., Hirao, H., Ito, T., Kadono, K., Dery, K. J., Kojima, H., Gjertson, D. W., Sosa, R. A., Kujawski, M., Busuttil, R. W., Reed, E. F., and Kupiec-Weglinski, J. W. (2020) Hepatic CEACAM1 expression indicates donor liver quality and prevents early transplantation injury. *J. Clin. Invest.* **130**, 2689–2704

79. Mantovani, A., Byrne, C. D., Bonora, E., and Targher, G. (2018) Nonalcoholic fatty liver disease and risk of incident type 2 diabetes: A meta-analysis. *Diabetes Care* **41**, 372–382

80. Russo, L., Muturi, H. T., Ghadieh, H. E., Ghanem, S. S., Bowman, T. A., Noh, H. L., Dagdeviren, S., Dogbey, G. Y., Kim, J. K., Heinrich, G., and Najjar, S. M. (2017) Liver-specific reconstitution of CEACAM1 reverses the metabolic abnormalities caused by its global deletion in male mice. *Diabetologia* **60**, 2463–2474

81. Fang, X., Yu, S. X., Lu, Y., Bast, R. C., Jr., Woodgett, J. R., and Mills, G. B. (2000) Phosphorylation and inactivation of glycogen synthase kinase 3 by protein kinase A. *Proc. Natl. Acad. Sci. U. S. A.* **97**, 11960–11965

82. Hermida, M. A., Dinesh Kumar, J., and Leslie, N. R. (2017) GSK3 and its interactions with the PI3K/AKT/mTOR signalling network. *Adv. Biol. Regul.* **65**, 5–15

83. Wu, D., and Pan, W. (2010) GSK3: A multifaceted kinase in Wnt signaling. *Trends Biochem. Sci.* **35**, 161–168

84. Gugiu, G. B. (2017) Lipid identification by untargeted tandem mass spectrometry coupled with ultra-high-pressure liquid chromatography. *Methods Mol. Biol.* **1609**, 65–82

85. Jin, L., Li, Y., Chen, C. J., Sherman, M. A., Le, K., and Shively, J. E. (2008) Direct interaction of tumor suppressor CEACAM1 with beta catenin: Identification of key residues in the long cytoplasmic domain. *Exp. Biol. Med. (Maywood)* **233**, 849–859